



# Benchmarking passive microwave satellite derived freeze/thaw datasets

Annett Bartsch<sup>1</sup>, Xaver Muri<sup>1</sup>, Markus Hetzenecker<sup>2</sup>, Kimmo Rautiainen<sup>3</sup>, Helena Bergstedt<sup>1</sup>, Jan Wuite<sup>2</sup>, Thomas Nagler<sup>2</sup>, and Dmitry Nicolsky<sup>4</sup>

<sup>1</sup>b.geos, Industriestrasse 1, 2100 Korneuburg, Austria

<sup>2</sup>ENVEO, Innsbruck, Austria

<sup>3</sup>FMI, Helsinki, Finland

<sup>4</sup>University of Alaska Fairbanks, Fairbanks, 99775, USA

**Correspondence:** Annett Bartsch (annett.bartsch@bgeos.com)

**Abstract.** Satellite derived soil surface state has been identified to be of added value for a wide range of applications. Frozen versus unfrozen conditions are operationally mostly derived using passive microwave (PMW) measurements from various sensors and different frequencies. Products differ thematically as well as in spatial and temporal characteristics. All of them offer only comparably coarse spatial resolution in the order of several km to tens of km which limits their applicability. Quality assessment is usually limited to comparisons with in situ point records, but a regional benchmarking dataset is thus far missing. Synthetic Aperture Radar (SAR) offers high spatial detail and thus is potentially suitable for assessment of the operational products. Specifically, dual polarized C-band data acquired by Sentinel-1, operating in Interferometric Wide (IW) swath mode with a ground resolution of 5 x 20 m in range and azimuth, provide dense time series in some regions and are therefore suitable as basis for benchmarking. We developed a robust freeze/thaw (FT) detection approach, applying a constant threshold on the combined C-band VV and VH polarization ratios, that is suitable for tundra regions. The achieved performance (91.8%) is similar to previous methods which apply an empirical local threshold on single polarized VV backscatter data.

All global products, tested with the resulting benchmarking dataset, are of value for freeze/thaw retrieval, although differences were found depending on seasons, in particular during spring and autumn transition. Fusion can improve the representation of thaw and freeze-up, but a multi-purpose applicability cannot be obtained since the transition periods are not fully captured by any of the operational coarse resolution products.

## 1 Introduction

Soil surface state (frozen or unfrozen) can be obtained from space using active and passive microwave (MW) data. Using spaceborne passive microwave data 42% of the northern hemisphere land surface has been identified to be affected by seasonal freezing and thawing (Kim et al., 2012). This includes permafrost regions, where it is a characteristic of the so-called active layer, the upper soil on top of permafrost. Satellite derived freeze/thaw (FT) information is hence suitable as proxy for permafrost characteristics (extent Park et al. (2016b), ground temperature Kroisleitner et al. (2018)). The performance of passive microwave retrieval algorithms depends on wavelength, acquisition timing, and the algorithm used to derive the surface state



(Johnston et al., 2020). Landcover at sub-grid scale needs to be considered in addition (Bergstedt and Bartsch, 2017; Bergstedt et al., 2020b).

25

A traditional application area of FT products is the masking of satellite derived soil moisture targeting a separation of periods with and without the presence of liquid water in the upper soil. The requirements are in such cases usually aligned with the soil moisture product (spatial and temporal resolution). However, some of the available products lack consistent FT flagging (Trofaier et al., 2017). Further potential of soil FT products includes for example assessment of the vegetation growing season (Kim et al., 2014, 2020; Park et al., 2016c; Böttcher et al., 2018), evapotranspiration (Zhang et al., 2021; Kim et al., 2018) and fluxes of greenhouse gases (Tenkanen et al., 2021; Erkkilä et al., 2023). The latter includes confining the activity period of soil microbes (Bartsch et al., 2007; Kim et al., 2014) and the combination with greenhouse gas concentrations derived from satellites and permafrost (Park et al., 2016a; Kroisleitner et al., 2018).

30

35

Different applications have different needs regarding FT detection. E.g for the climate modelling community a frozen fraction approach is required rather than a frozen/unfrozen classification (Bergstedt et al., 2020b). Subgrid information of snowmelt patterns are also of interest in the context of long-term ecosystem monitoring in the Arctic (Rixen et al., 2022). Surface state products derived by satellites represent either the surface condition of snow and ice or soils. In case of snow the terms 'wet/dry' or 'frozen/melting' are used, while for soil the terms 'frozen/unfrozen' are used to describe the states. Dedicated FT products mostly address soils and thus acquisitions under snow-free conditions, but wet snow information is of added value for such observations due to associated changes in soil temperature beneath the snow pack (e.g. Bartsch et al., 2007; Kroisleitner et al., 2018). Climate change impact can be documented through the length of the unfrozen/snow-free season, but spring snow thaw timing and length of snow melt period needs to be monitored in addition (e.g. Kouki et al., 2019).

40

45

The production of a FT Climate Data Record (CDR) may require the combination of products from different satellites. Differences between records using different wavelengths have been identified (e.g. Johnston et al., 2020). A range of strategies for fusion of different records have been proposed, specifically L-band passive microwave and C-band scatterometer (Chen et al., 2019; Zhong et al., 2022). Inconsistencies and systematic differences due to acquisition timing and differences regarding wavelength and system (active – passive; Trofaier et al., 2017, static in the beginning, varying towards the end) need further investigation. The utility of the products varies not only based on different user needs but also on the retrieval approach and calibration data. Reanalyses data are commonly used to define a threshold for surface state classification. 0°C is applied as threshold for passive records representing the brightness temperature and reanalysis values relationship through a cosine function (Kim et al., 2014). Naeimi et al. (2012) fit a logistic function to describe a temperature - C-VV backscatter relationship. The turning point of the function is considered as threshold. Kroisleitner et al. (2018) found that the PMW derived frozen period length differs considerably from Naeimi et al. (2012). Possible reasons are the acquisition time, wavelength and calibration approach. These approaches differ from snowmelt products where for example in case of sea ice a temperature above -1°C for 3 consecutive days is considered (Smith et al., 2022). Over land, diurnal thaw and refreeze as condition for

50

55



start of spring melt has been suggested alternatively, but this requires higher repeat measurement intervals than usually available (Bartsch et al., 2007). Most products target 80% detection accuracy. A commonly agreed benchmark for this assessment is lacking so far relating partially to lack of representation of spatial variations by the available in situ data within the footprints.

Consolidated requirements for a FT product aiming at permafrost research have so far only been stated in Bartsch et al. (2022). A 100m spatial resolution product in 10 day intervals has been requested. Kroisleitner et al. (2018, with focus on Metop ASCAT and SSMI) exemplify that daily resolution is required for ground temperature estimation. General requirements for a ground temperature product have been collected as part of the Permafrost\_cci baseline project (Bartsch et al., 2023e) which need to be considered in this context. As a threshold requirement for temporal and spatial coverage, at least the last decade needs to be addressed as well as the whole Arctic. The target should be a global product. 10 km (threshold) and 1 km (target) resolution respectively are eventually needed to serve the needs of permafrost modelling at global scale (Bartsch et al., 2023e).

A major challenge of coarse resolution satellite products from PMWdata across the Arctic is the quality assessment with in situ data due to the scarce availability of ground stations and loss of representativeness because of high landscape heterogeneity. Available FT products have a nominal spatial resolution in the order of several tens of kilometres. Bergstedt et al. (2020b) demonstrated that considerable variations can occur within a footprint due to topography and/or variability in land surface types. Another option for evaluating the quality of coarse resolution products is by using data based on C-Band which have a higher spatial resolution. So far such investigations have been limited to C-band scatterometer, specifically Metop Advanced Scatterometer (ASCAT).

A strategy for a SAR-based benchmark dataset creation which relies on calibration with reanalyses data is described in Bergstedt et al. (2020b). This calibration approach follows the methodology proposed for scatterometer by Naeimi et al. (2012). It needs to be carried out for each footprint/pixel individually since various factors, such as surface roughness and volume scattering in the surface layer, may impact the absolute backscatter intensity values. Naeimi et al. (2012) compared gridded temperature data (ERA-Interim reanalyses data) and Metop ASCAT C-Band VV backscatter data (grid spacing appr. 12.5km) and fitted a logistic curve. The lower flat part of the function represents frozen conditions, while the upper flat part relates to the unfrozen conditions. The inflection point provides the location specific threshold. This method requires suitable temperature data for each grid point. As this not available at high spatial resolution as provided by Sentinel-1 (5 x 20 m; 10m nominal resolution) a method independent from such parameterization needs to be developed for regional applications. An algorithm which for example makes use of a universal threshold is required. The study by Bergstedt et al. (2020b) was in addition limited to VV polarization matching ASCAT properties. Backscatter intensity expressed as  $\sigma_0$  was used and incidence angle normalization to 40 degree was applied using the approach by Widhalm et al. (2018) in order to match ASCAT specifications. An overall accuracy of 94% was obtained in comparison to soil temperature data from a tundra area. Missions such as Copernicus Sentinel-1 operate in dual polarization mode, providing co- and cross-polarization over most land areas (commonly VV and VH). The use



of both for FT has been investigated only in very few cases so far. Cohen et al. (2021) calculate the backscatter difference (of each to be classified date) with respect to a frozen and unfrozen reference (pre-selected representative scenes). The study was eventually also limited to VV as the focus was on forested environments where VH is expected to be influenced by the canopy.  $\sigma_0$  was used and ground and canopy contribution separated (including consideration of incidence angle). A static, but regional specific threshold applied to the difference between the deviation from the frozen and thawed reference respectively is suggested. Similarities with air temperature was between 64% and 99% depending on region. A further approach which has been regionally tested for Sentinel-1 is the use of a convolutional neural network (CNN) algorithm trained also using backscatter from a frozen and unfrozen reference period, using both VV and VH, plus incidence angle and landcover information (Chen et al., 2024). A classification accuracy of 88% was obtained in comparison to soil temperature data across an area north of the treeline where the CNN was trained.

Algorithms exist which use backscatter ratios for wet/dry snow detection based on Sentinel-1. This allows the application of a global threshold value to distinguish between states without a location specific parameterization also avoiding the need to directly consider the incidence angle (Nagler and Rott, 2000). The scheme has so far not been tested for soil FT. Previous calibration and validation activities have found that a global threshold of -2 dB (ratio between acquisition and reference image) is suitable to discriminate wet and dry snow. It is hypothesized that a similar strategy is suitable for frozen versus unfrozen soil classification. This requires sites with good in situ data availability which are scarce in permafrost regions. A comparably high number of borehole records is, however, available over the Alaskan North Slope (Biskaborn et al., 2019). Also, measurements from a FT dedicated sensor network are available from Northern Finland (Bergstedt et al., 2020b).

The purpose of this study is to evaluate the utility of C-band SAR data available at VV and VH polarizations for benchmarking of passive microwave satellite derived freeze/thaw products which have coarse resolution but global coverage. In situ air as well as soil temperature from different locations across the Alaskan North Slope are used to identify a suitable ratio threshold for the benchmark dataset creation. Validation includes near surface soil temperature records from Northern Finland. The focus is on tundra areas and the evolution of thaw and freeze-up within the footprint of the coarse resolution products and the discussion of implications of differences between the datasets for a range of potential applications.

## 2 Data and analyses regions

### 2.1 Available global/northern hemisphere products

Three FT datasets based on relatively coarse spatial resolution PMW information are considered for benchmarking (Table 1). The currently listed FT Fundamental Climate Data Record (FCDR) in the WGClimate catalog is the MEaSURES Global Record of Daily Landscape Freeze/Thaw Status, Version 3 (Kim et al., 2014) which is associated to the ECV (Essential Climate Variable) soil moisture. It is based on various passive microwave missions (SMMR, SSM/I, and AMSR-E) and goes back to



**Table 1.** Freeze/thaw datasets with northern hemisphere coverage considered for benchmarking with Sentinel-1 retrievals

Dataset name	Sensor(s)/Mission(s)	Start date	Gridding	Flags
MEaSURES	SMMR, SSM/I, and AMSR-E	1979	25km	Frozen, unfrozen
Soil Moisture Active and Passive mission	SMAP	2015	9km	Frozen, unfrozen
Soil Moisture and Ocean Salinity mission	SMOS	2010	25km	Frozen, unfrozen, thawing

1979. It is provided with 25km gridding, separation of AM and PM, and >80% mean annual spatial classification accuracy. FT information is supplied binary (either frozen or unfrozen). Vegetation related use of the product is suggested apart from soil moisture masking (<https://climatemonitoring.info/ecvinventory/>). An updated version (version 5) is currently available through the National Snow and Ice Data Center (NSIDC; Kim et al. (2017, 2021)). The same input data sets are also considered for directly deriving landsurface temperature for the production of climate records within the ESA LST\_cci project (Dodd et al., 2021). The AMSR-E/AMSR2 based time series integrated in the NASA MEaSURES program is a 6 km resolution record covering the northern and southern hemisphere currently spanning the period 2002-2020 (Kim et al., 2021). AM and PM measurements are fused for a daily product. The nominal resolution results from gridding of AMSR-E/AMSR2 native footprints of 14km x 8km and 12km x 7km respectively (Kim et al., 2021). Binary FT information is available.

135

Further products exist from SMAP (2015-) and SMOS (2010-) provided on an operational basis (Kraatz et al., 2018; Rautiainen et al., 2016). Both are L-band PMW missions and provide therefore information on the upper centimeters of the soil. The SMAP mission specifically targets freeze/thaw, complementing soil moisture, and requirements have been defined for the mission (Dunbar, 2018; Entekhabi et al., 2014). They have been phased for the radar instrument (which is currently not in operation). Surface binary freeze/thaw state in the region north of 45°N latitude, which includes the boreal forest zone, was targeted with a classification accuracy of 80% at 3 km spatial resolution and 2-day average intervals. A two-day precision at the spatial scale of landscape variability ( $\approx 3$  km) was originally targeted. The available SMAP PMW product considers four stages: frozen, thawed, transitional, inverse transitional. The two transitional categories refer to days with differences between AM and PM acquisitions. The passive microwave product shows >70% accuracy with 36 km gridding (Kraatz et al., 2018). The SMOS mission FT product provides discrete classes and addresses three stages: thawed, partially frozen or frozen for the northern hemisphere (daily, 25km; (Rautiainen et al., 2016).

Several active microwave products have been published previously but are limited temporally and spatially and are thus not considered for benchmarking. These include an experimental product from Metop ASCAT (C-band scatterometer, 12.5 km gridding, Paulik et al. (2012)), starting in 2007, aimed at permafrost and flux applications (Naeimi et al., 2012). It is available for 12.5 km nominal resolution and considers three states: frozen, unfrozen, melting. In addition, a C-band SAR product at 1km has been developed based on ENVISAT ASAR GM (Park et al., 2011) and is used to assess the ASCAT product (Bergstedt and Bartsch, 2017).



## 2.2 Sentinel-1

155 The Copernicus Sentinel-1 C-band SAR mission consisted of two satellites for the analysis period 2014 to 2020. Sentinel-1A was launched in April 2014 and Sentinel-1B followed in April 2016. In order to provide global coverage, Sentinel-1 mission is operating in a 12 days repeat cycle over most land surfaces, however, it is operated over Europe and selected other regions with a 6 days repeat cycle using 2 satellites.

The capability of Copernicus Sentinel-1 for FT products has been demonstrated e.g. by Bergstedt et al. (2020b) and Cohen et al. (2021). The primary data source for the benchmarking is therefore Sentinel-1 C-band SAR data acquired in IW Terrain Observation with Progressive Scans (TOPS) mode at VV and VH polarization. Acquisition types and coverage vary considerably across the Arctic (Bartsch et al., 2021a). The required data are unavailable for Greenland and the Canadian High Arctic (Bartsch et al., 2021b). Comparably good coverage is available for Alaska as well as Scandinavia. These areas overlap with in situ measurement sites relevant for this study. All scenes starting 30th of July 2017 to 31st of December 2020 have been processed for northern Alaska (covering all automatic weather stations and borehole locations, see Figure 1) and all scenes for August 2016 to August 2018 covering the Kaldoaivi area in Northern Finland (Figure 2). Benchmarking of the PMW datasets has been carried out over 17 SMOS grid cells (and overlapping SMAP and MEaSURES cells) over Alaska and 12 cells over Northern Finland.

## 2.3 Temperature records

170 Temperature records from in situ observations include long-term measurement sites such as boreholes and automatic weather stations (AWS) as well as short-term and spatially distributed observations using iButton data loggers. The latter network was established for validating surface conditions derived from C-band satellite data (for details see Bergstedt et al. (2020b)). They have been used for inter-comparing Sentinel-1 with a coarser regional dataset based on Metop ASCAT covering the region Kaldoaivi in Northern Finland. This site is located within a palsa mire and represents a zone of sporadic permafrost. The temperature sensors have been distributed in the proximity of a permafrost borehole site. The majority of the iButtons are located outside of permafrost affected landscape elements. The snow water equivalent (SWE) varies across the sites in winter, but at most sites snow depth is sufficient for insulation and temperatures remain close to 0°C below the snowpack. The available record includes 24 sites spanning two years (August 2016 to August 2018). The iButton loggers were placed approximately 2–3 cm below the surface to avoid direct warming influence by the Sun.

180 Records from boreholes and AWS across Alaska including the North Slope, representing continuous to discontinuous permafrost, have been used for calibration (Figure 1). Data is available from 26 boreholes with depths varying between 1-75 cm and from 22 AWS providing air temperature. Three years of data (2018 to 2020) have been used. ERA5 reanalyses data for the same time period were used in addition for the evaluation of the fused dataset to allow comparability with previous studies.

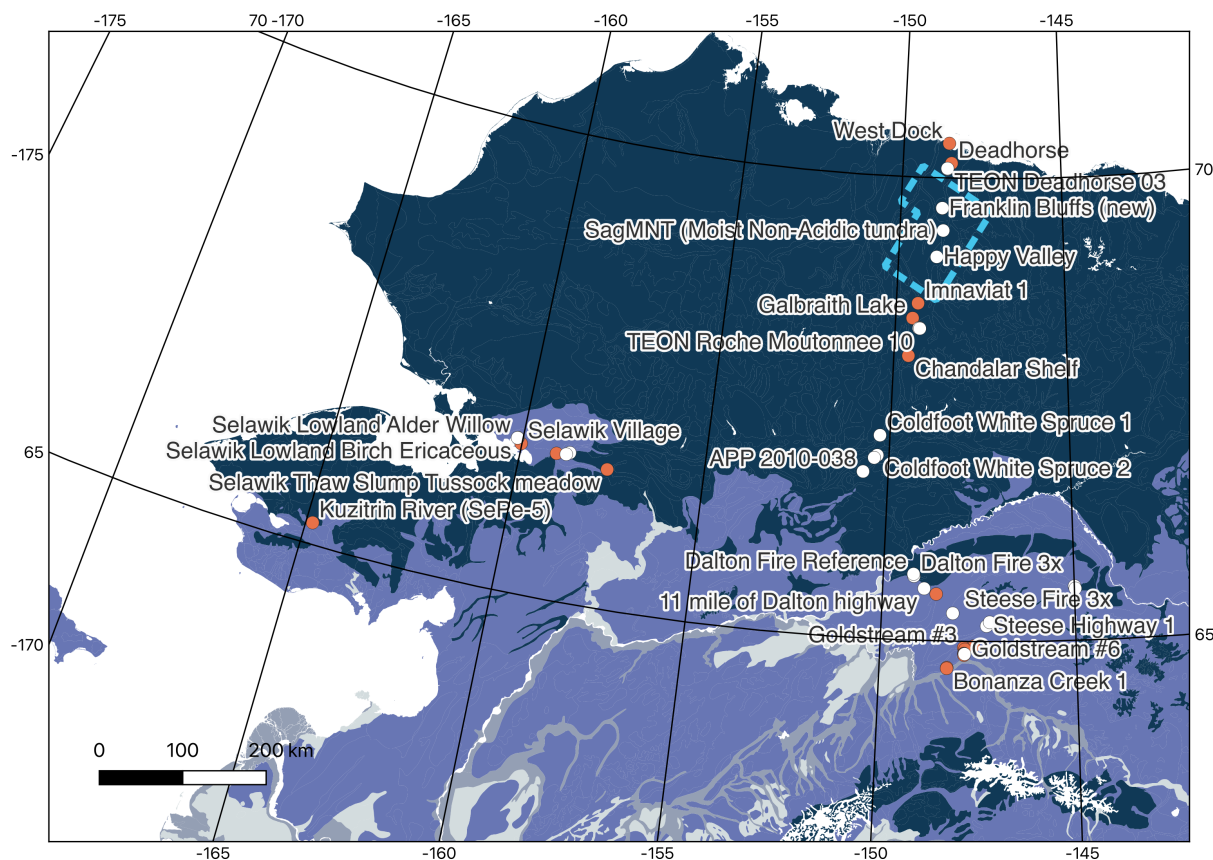


**Figure 1.** Location of in situ data sites with air (red) and soil (white) temperature for 2018 to 2020. Background: permafrost zones from Jorgenson et al. (2008), from dark to light blue: continuous, discontinuous, sporadic, isolated. Dashed outline indicates region for benchmarking and fusion.

**Table 2.** In situ datasets used for calibration and validation of the benchmark dataset creation, as well as for the fusion assessment.

Region	Instrumentation type	Data type	data points	time period	Use
Alaska, including North Slope	AWS	Air temperature	22	June 2018 - December 2020	calibration
Alaska, including North Slope	boreholes	soil temperature (closest to surface: 1-75cm, median 22 cm)	26	June 2018 - December 2020	calibration (all), fusion assessment with subset (three sites with sensors at 5-7 cm)
Northern Finland, including Kaldoaivi	iButtons	near surface soil temperature (2-3cm)	24	August 2016 - August 2018	validation

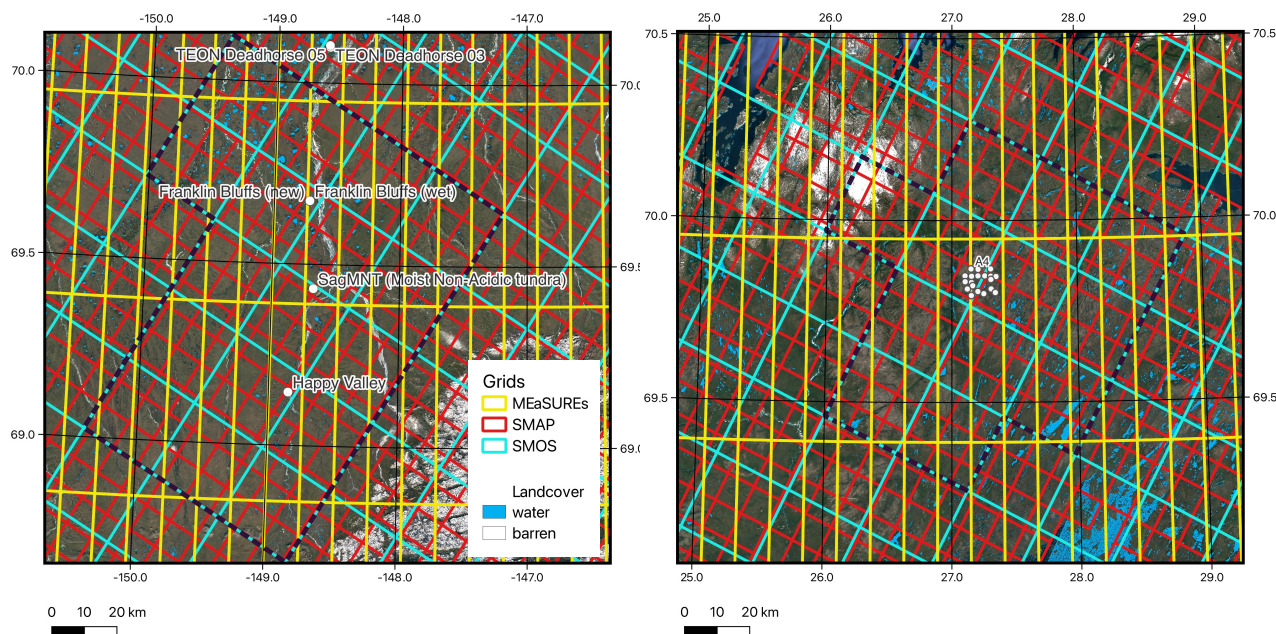


**Figure 2.** Examples of satellite product grids (see Table 1) for sites with in-situ borehole data on the Alaskan North Slope (left) and iButton data at Kaldoaivi, Northern Finland (right). Background: selected landcover classes relevant for masking (source: Bartsch et al. (2023c)) and Google hybrid. In situ sites shown as white filled circles. Black dashed lines indicate the boundary of SMOS cell extent used for assessment and fusion.

### 3 Methods

#### 185 3.1 General workflow

First, the benchmarking dataset was created using Sentinel-1. The implementation of surface state classification building on intermediate products of the wet/snow retrieval as proposed in Nagler and Rott (2000) requires a threshold determination in a first step. For calibration in-situ data from Alaska limited to the upper few centimeters of the soil have been used. The target landcover type (as determined by the potential applications of a FT product) are soils. Water surfaces, bare areas and glaciers therefore need to be masked with a dataset of similar spatial resolution (Bergstedt et al., 2020b). The circumpolar landcover units by Bartsch et al. (2023d) fulfil this requirement and have therefore been used for masking.

Eventually, the frozen fraction is derived individually (spatial subsetting) from the masked data for each cell of the PMW FT products listed in Table 1. The resulting time series are used for the evaluation and the development of the fusion scheme. Fused records are assessed with the benchmark dataset similarly as the input records as well as with in-situ records. The fused record examples are combined with a dataset providing mid-winter thaw and refreeze of snow (Bartsch et al., 2023a), where such events occur, to facilitate the discussion.



### 3.2 Pre-processing of SAR data

The original wet/dry snow detection utilizes repeat pass dual-pol Copernicus Sentinel-1 SAR data (acquired in IW swath mode) from different tracks. The method includes the generation of reference images, applying a statistical pixel-wise analysis of tens of co-registered repeat pass Sentinel-1 images Nagler et al. (2016). To exploit the dual-polarisation capabilities of Sentinel-1 the backscatter ratio of the snow covered period and reference data are calculated separately for co- and cross-polarisation and then combined. The combination accounts for differences in angular backscatter behaviour of co- and cross-polarized backscatter data by applying the local incidence angle as weighting factor. The result is a weighted ratio combination  $R_C$  (Nagler et al., 2016).

More than 1900 scenes have been pre-processed in total over both regions. In situ locations in Alaska were covered by 52 to 179 scenes each. 115 scenes have been used over Finland for comparison with in-situ records. The time period covered for Finland corresponds with the in-situ data availability (August 2016 to August 2018, acquisitions every 12 days). Data processed for Alaska span three years from 2018 to 2020 (on average an acquisition every 9 days using overlapping orbits).

### 3.3 Freeze/thaw retrieval from SAR data and evaluation

The last step of the wet snow retrieval scheme of Nagler et al. (2016) is the segmentation of wet snow versus snow-free and dry snow areas based on the backscatter ratios of VV ( $R_{VV}$ ) and VH ( $R_{VH}$ ) which are combined as  $R_C$  images Nagler et al. (2016). This step was adjusted for the FT retrieval. Specifically, a suitable threshold  $Thr$  needed to be defined for the segmentation of frozen versus unfrozen soil.

The threshold determination followed the approach originally suggested for VV backscatter time series by Naeimi et al. (2012) (Scatterometer) and adapted by Bergstedt et al. (2020b) (SAR). The threshold is defined based on a logistic function fit between backscatter and temperature data and the threshold  $Thr$  determined from the inflection point. This was based on reanalyses data in the past studies. Here we used in situ data instead. Air temperature as well as soil temperature measurements were considered. The inflection point of the fitted function was derived for both types and the corresponding backscatter value used as threshold to distinguish between frozen (less equal  $Thr$ ) and unfrozen (greater  $Thr$ ) conditions. Here, we apply it to the combined VV and VH ratio values ( $R_C$ ) as defined in (Nagler et al., 2016). The logistic function has been defined based on the processed  $R_C$  data on the Alaskan North Slope. The fitting procedure includes the consideration of the maximum value of  $R_C$  and the average for all values acquired under conditions below  $-5^{\circ}\text{C}$ . For the borehole records the upper most sensor below the ground has been selected. Validation of the threshold approach was carried out based on the near surface temperature observations available for Northern Finland (Kaldoaivi). For this purpose, daily averages of  $0^{\circ}\text{C}$  and lower are defined as frozen and all values above as unfrozen.

A disadvantage of using backscatter intensity at C-VV is the temperature dependence at cold conditions (Naeimi et al., 2012; Bergstedt et al., 2020b; Bartsch et al., 2023b). The potential influence was therefore also investigated using the available in situ records. In addition to  $R_C$ , C-VV and C-VH backscatter intensity input values were compared with the temperature



230 measurements.

### 3.4 Sub-setting global and fused dataset records for evaluation

The available global products represent varying grids. Therefore, the Sentinel-1 backscatter ratio analyses needed to be carried out over sufficiently large areas in the proximity of the in-situ locations (overlap of grids, Figure 2). Permanent snow and ice covered areas, water and barren (bedrock) have been extracted from landcover for the masking of 'none-soil'. The 'none-soil' fraction can be very large in permafrost environments. Figure 2 shows lakes and bare area as derived from a landcover map (Bartsch et al., 2023c) for the Alaskan North Slope. Both landcover types were excluded from the frozen fraction calculations.

The frozen/unfrozen fraction was derived for each of the overlapping footprints. The spring and autumn transition zone was considered in addition to the unfrozen period where available. Basic statistics were derived for each global product separately (including for the presentation of results as violin plots).

### 3.5 Fusion: scheme and evaluation

Criteria for preference of a certain dataset were eventually defined for a fusion scheme based on the benchmarking. The year is split into three phases for this purpose: DOY (day of year) 1 - 209, 210-300, and >300. In a first step, dataset(s) to be considered for a certain period were selected. In a second step the conditions were defined (considering agreement between datasets/results of benchmarking). The combined dataset (referred to as Fusion) was eventually also compared to the benchmark dataset derived from the Sentinel-1 frozen fraction. All comparisons of the Fusion dataset were made on the basis of the SMOS grid as the new grid. The 'partially frozen' flag was separately analyzed from the other flags.

Data from three borehole locations on the Alaskan North Slope were used for the assessment of the unfrozen and frozen flags (temperature sensors at 5-7cm depth) of the fusion product. In addition, ERA5 reanalysis data (air temperature) were investigated at the same sites (for location see Figure 2). The frozen state retrieval from the soil and ERA5 temperature data was based on the following temperature thresholds: values  $< -1^{\circ}\text{C}$  are considered as frozen and values  $> 1^{\circ}\text{C}$  as unfrozen, while values in between are classified as partial thaw.

Days with mid-winter thaw and refreeze of the snowpack or wet snow were not part of the benchmarking but can also be potentially added using existing products. As an example, mid-winter thaw and refreeze as available from fusion of Metop ASCAT and SMOS (Bartsch et al., 2023b) has been added and an own flag value assigned. Such data are applicable for November to February (day of year 300 to 60).

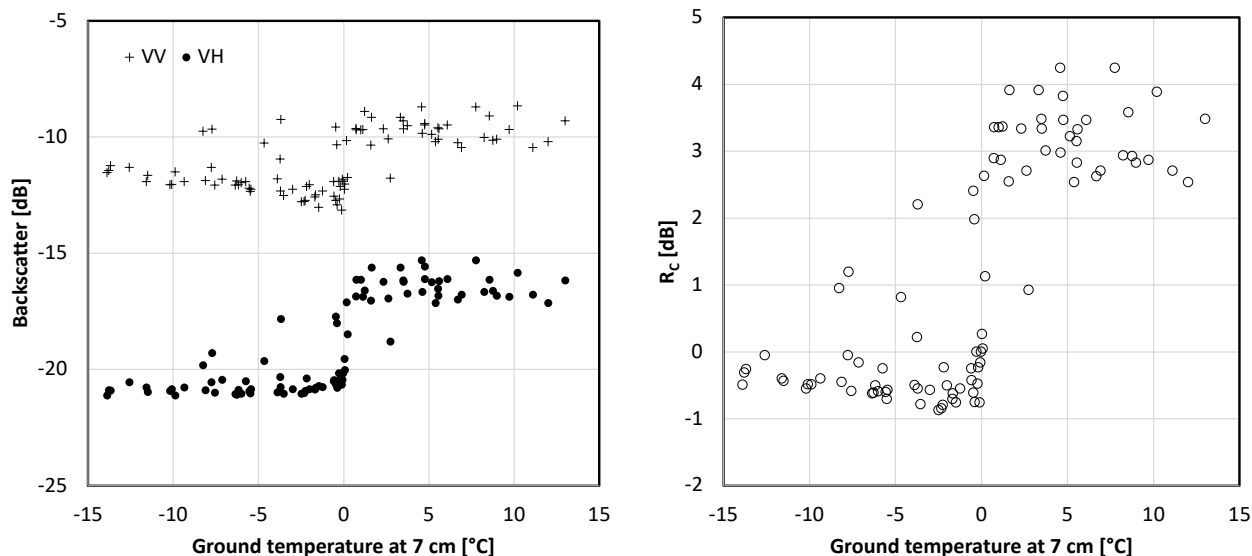


**Figure 3.** Sentinel-1 backscatter intensity at VV and VH as well as combined ratios  $R_C$  (92 acquisitions) versus daily sub-ground temperature (7 cm depth, 5 June 2018 to 27 December 2020) at Sagwon (SagMNT, Alaska). For location see Figure 1).

## 260 4 Results

### 4.1 Temperature effect

The temperature influence on C-VV backscatter as described in Bergstedt et al. (2020b) and Bartsch et al. (2023b) does not apply to VH (Figure 3). Backscatter remains at a similar level for all temperatures below 0°C at this polarization combination. Differences between the years due to changes in snow structure, as can especially occur due to rain-on-snow events (Bartsch et al., 2023b), are also less pronounced at VH. The temperature influence is visible in the combined VV and VH ratio values ( $R_C$ ; increasing backscatter with decreasing temperature), inherited from VV, but the magnitude is lower than in the VV input data.

### 4.2 Sentinel-1 threshold determination and validation

The determined value of the inflection point from the logistic function fitting varies across sites (examples for comparison with soil temperature in Figure 4). The spread of the ratio values in winter as well as summer is large, in the order of one to two, but they are largely distinct.

Only minor differences are found between results using soil temperature and air temperature data (Figure 5). The mean values of the inflection point differ by only 0.12 dB. The range is higher for air temperature. All values are higher than the suggested threshold for wet snow (-2dB, Nagler et al. (2016)). Most inflection point values even exceed it by more than 3 dB.

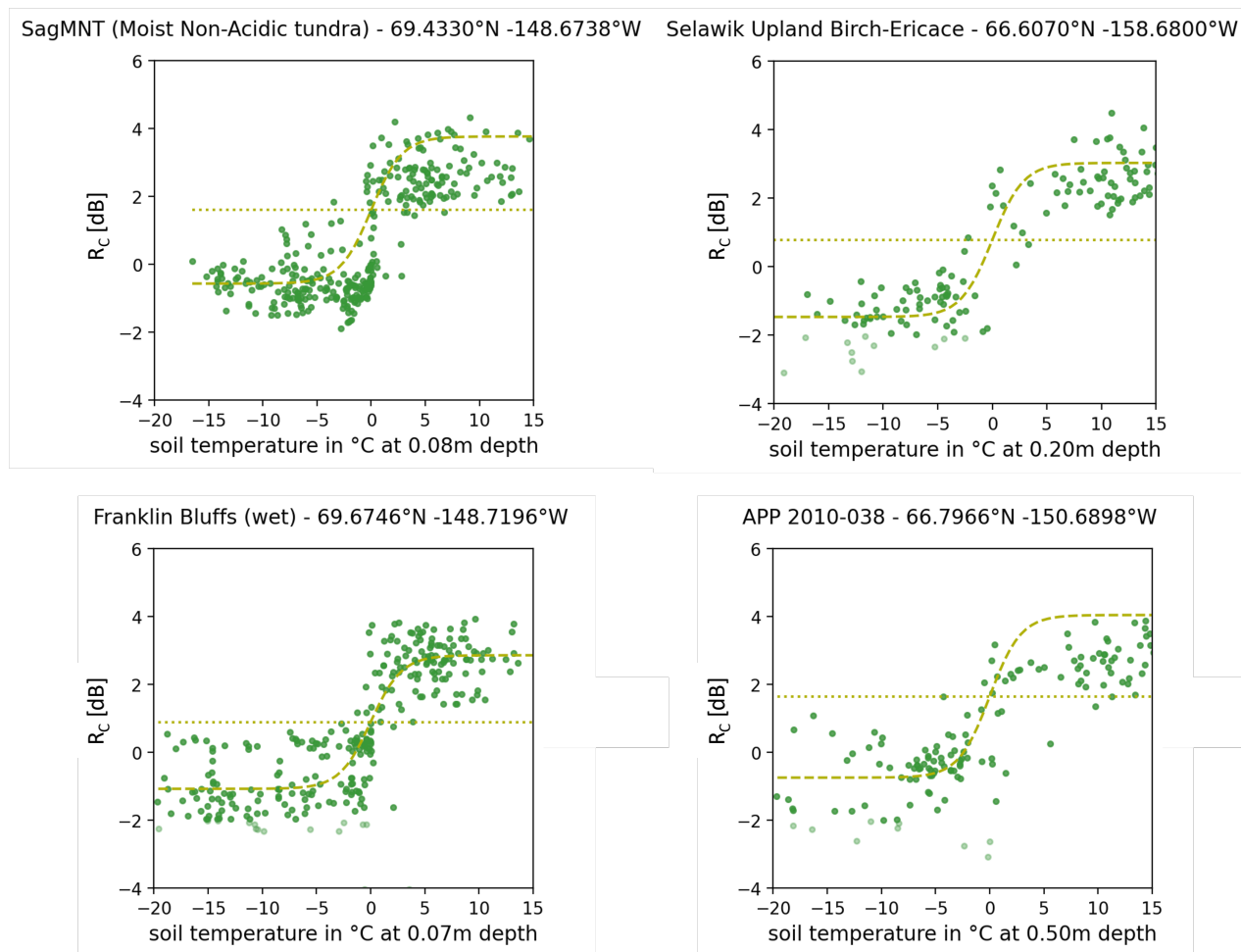


**Figure 4.** Examples for threshold determination at four borehole sites. Sentinel-1 combined polarization ratios ( $R_C$ ) and in-situ soil temperature are compared. Light green indicates  $R_C$  values below the wet/dry snow threshold (as defined in Nagler et al. (2016)) Dashed line – fitted function. Dotted line – determined inflection point. For location of sites, see Figure 1).

275 A threshold of 1.34 based on the soil data (median) is suggested for regions with a soil layer that can contain water/ice (basic requirement for FT detection).

The applicability of the threshold could be confirmed using independent records, by use of the in situ data from Northern Finland (Kaldoaivi region, see Table 2). In total more than 1800 samples of daily average temperature from 24 sites have been available for the Kaldoaivi region. 93.2% of all samples within the two year time period were correctly classified for unfrozen conditions, and 91.2% of the frozen conditions (average 91.8%).

280

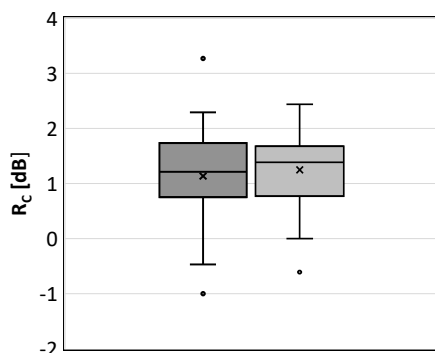


**Figure 5.** Sentinel-1 combined polarization ratios ( $R_C$ ) statistics (boxplots) of inflection points of the logistical function fitted to temperature data following the threshold detection method of Naeimi et al. (2012) (air and soil temperature, 26 and 22 samples respectively; in-situ record overview in Figure 1).

### 4.3 Freeze/Thaw fraction within PMW grids

Only grid cells of the PMW datasets that are completely covered by the Sentinel-1 scenes have been cross-compared (Alaska: Figure 6; Finland: Figure 7). The shown results are limited to two periods: April to June (from completely frozen to completely unfrozen) and August to November (from completely unfrozen to completely frozen) in order to identify potential issues for the different transition types. Violin plots have been chosen to visualize the data distribution (of frozen fraction) for thawed and frozen conditions as defined in the products. For SMOS, the fraction was also analysed for the 'thawing' flag which represents partially unfrozen conditions. Time series examples are provided for two distinct borehole locations, Happy Valley and Sagwon (Figure 8). The frozen flags of each product were translated into values of 10 (unfrozen), 20 (partially frozen) and 30 (frozen) for comparability in these cases. Near surface soil temperature and frozen fraction are shown together with the new flag values. In spring, the frozen fraction as detected by Sentinel-1 drops when the in situ temperature (1 cm depth) starts to rise above the late winter level at Happy Valley. This drop does not coincide with the beginning of the thaw in the PMW cells. The start of frozen fraction increase does, however, agree with the drop below 0°C in the 2020 example. This is similar for the second site (Sagwon, 8 cm depth, Figure 8). Both borehole records show the so called zero curtain effect at freeze-up. Temperatures can remain at almost 0°C for weeks to months due to latent heat which maintains the temperatures (Outcalt et al., 1990). The frozen fraction is already at 100% weeks before the ground temperature eventually lowers.

The fraction comparison clearly shows a frozen state detection issue for SMAP during the winter on the Alaskan North Slope (Figure 6). A higher number of grid cells is defined as unfrozen than for the other datasets. This effect is more pronounced for April to June than for August to November. This leads to a premature thaw detection in spring. The timing of complete freeze-up is, however, in general captured when the flag switches from unfrozen to frozen as can be demonstrated for the Happy Valley borehole location for 2020 (Figure 8). The unfrozen flag is assigned to the SMAP grid cell from the beginning of the depicted time period, starting 1st of April 2020. The frozen fraction as determined by Sentinel-1 drops below 100% towards



**Table 3.** Summary of benchmarking results considering the target transition periods

Frozen	Thaw	Unfrozen	Freeze-up	frozen
winter issue SMAP	Start: best represented in MEaSURES  End: partially represented in SMOS	no issues	Start: partially represented in SMAP and MEaSURES  End: represented by SMAP	winter issue SMAP

the end of April and reaches 0% in June. The 'unfrozen flag' issue at Happy Valley returns mid November. This happens only occasionally at the Sagwon site (Figure 8). AMSR and SSMI flags switch from frozen to unfrozen by end of May when the  
 305 Sentinel-1 frozen fraction is at almost 0%. The 'partially frozen' flag in SMOS only occurs here in autumn (coinciding with a frozen fraction of about 80%) what can also be shown for a further borehole location for autumn transition in 2019 (Sagwon, Figure 8) and agrees with the fraction comparison results from the North Slope (Figure 6).

SMOS captures the mid to finalization of thaw on the North Slope well and is closer to the start of thaw for Northern Finland  
 310 (unfrozen flag includes a higher fraction of frozen conditions, Figure 7). Freeze-up is detected with a delay. The majority of days with partially thawed flag show almost complete freeze-up (spatially) in Sentinel-1. The MEaSURES AMSR-E and SSMI products largely agree with each other (time series examples Figure 8). The spring switch occurs at start to mid-thaw at the Happy Valley borehole location. The average frozen fraction with unfrozen flag in spring is lower than for the other products.

The benchmarking results suggest the need for a fusion of all available products (Table 3). This allows a start of the time  
 315 series in 2015 only (SMAP launch). The start and end of thaw can be represented back to 2010 (SMOS). The MEaSURES records back to 1979 allow good detection of the start to mid thaw.

#### 4.4 Suggested fusion scheme based on the benchmarking

SMOS and MEaSURES (SSMI or AMSR) are recommended to be considered in all three time periods (Table 4). The perfor-  
 320 mance of these products was shown to be similar for early winter, therefore either of the products can be used. For late winter and during the thaw period, differentiation needs to be made whether the different products agree with each other or not. SMAP is recommended to be considered for the definition of 'partially frozen' during freeze-up, specifically when its flags disagree with the other products.

325 The PMW were fused following the rules defined in commended to be considered in all three time periods and using the SMOS grid cell definition (see also figure 2). The previously introduced scheme for flag values (10 – unfrozen, 20 - partially frozen, 30 – frozen) was applied.

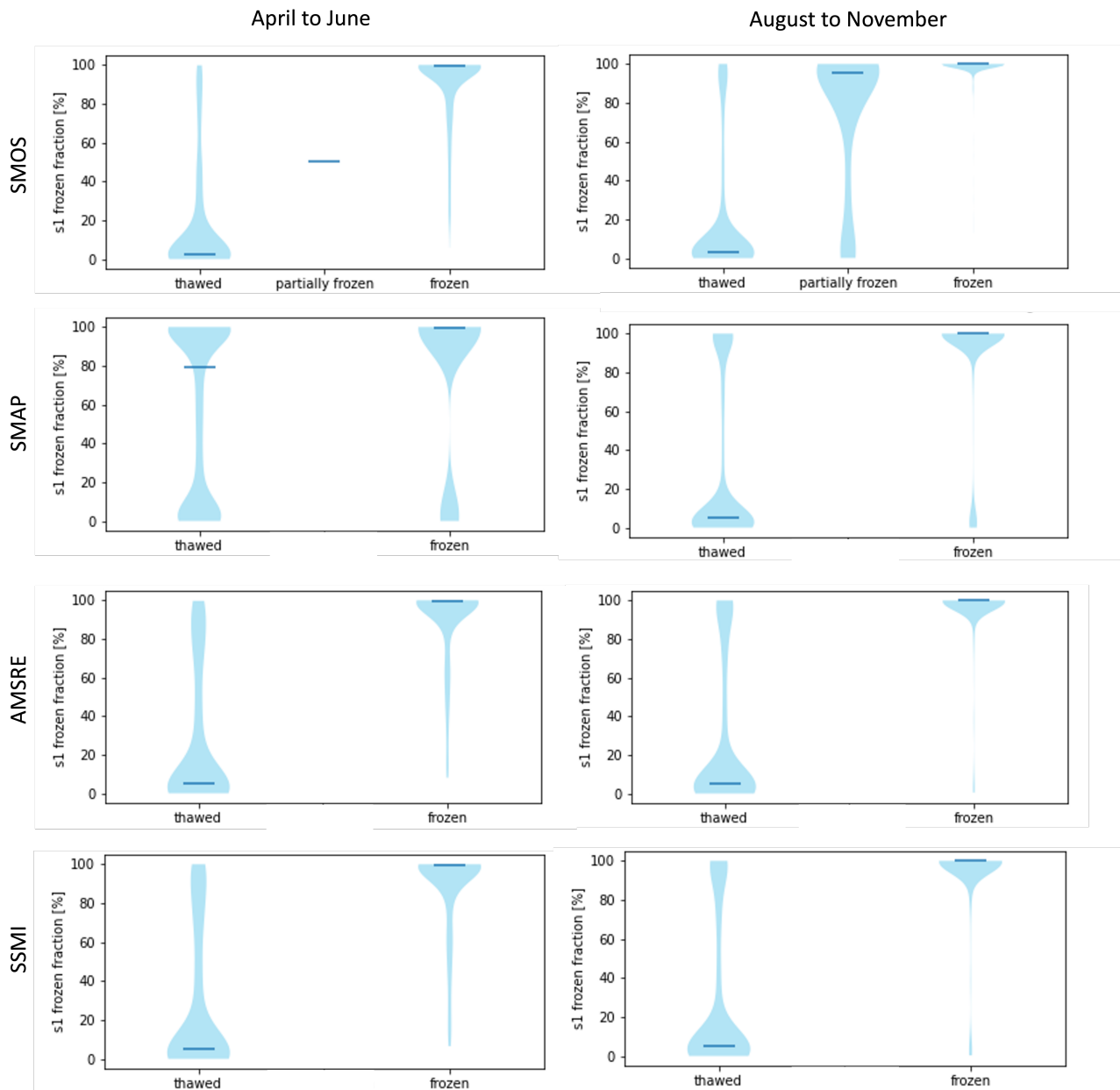


**Figure 6.** Sentinel-1 (s1) derived frozen fraction for footprints of SMOS, SMAP and MEaSUREs (AMSR and SSMI) freeze/thaw products. Sample period 2017 to 2020, Alaskan North Slope. For analyses extent see Figure 2.

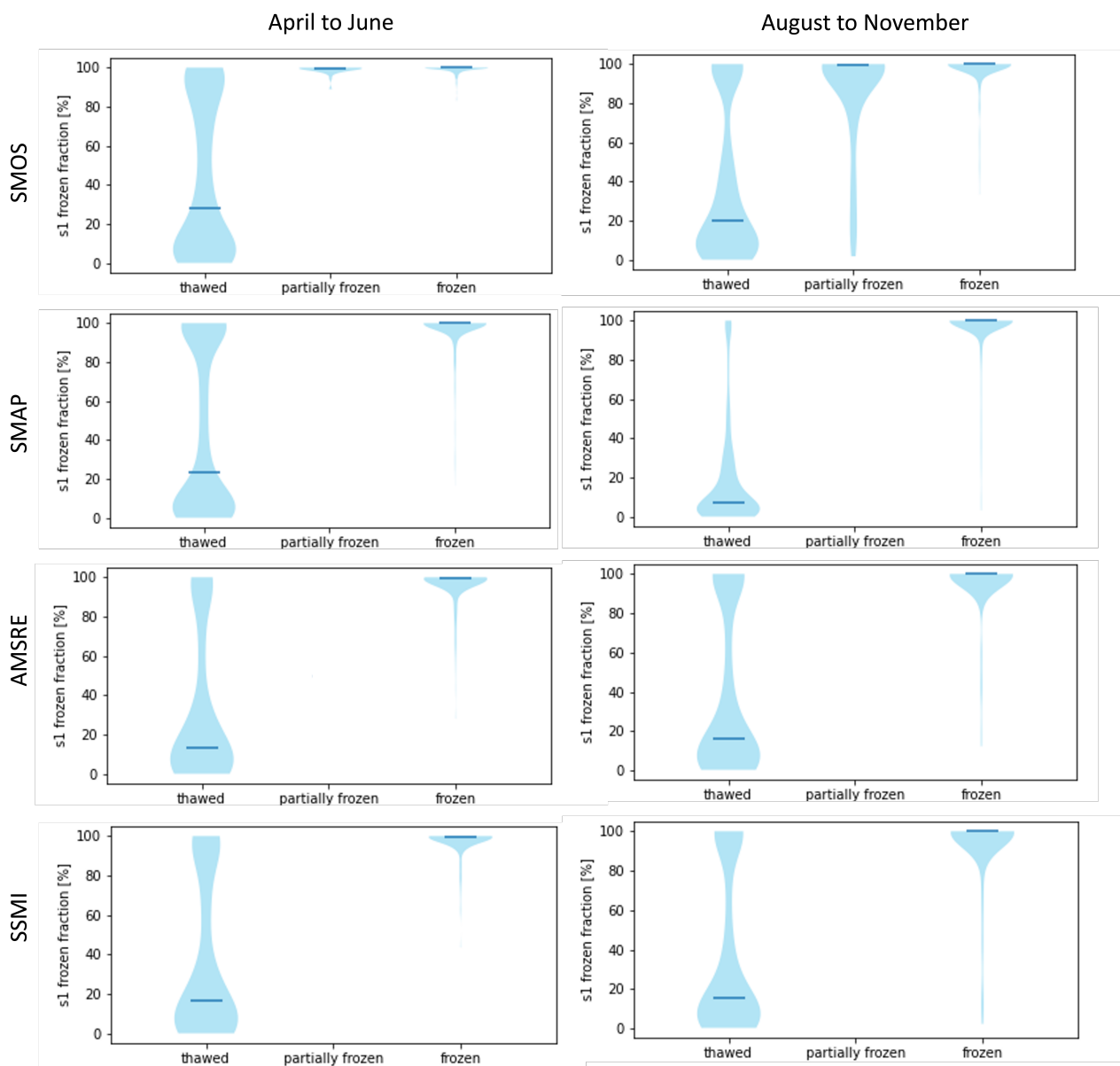


**Figure 7.** Sentinel-1 (s1) derived frozen fraction for footprints of SMOS, SMAP and MEaSUREs (AMSR and SSMI) freeze/thaw products. Sample period 2018 to 2020, Kaldoaivi, Northern Finland. For analyses extent see Figure 2.

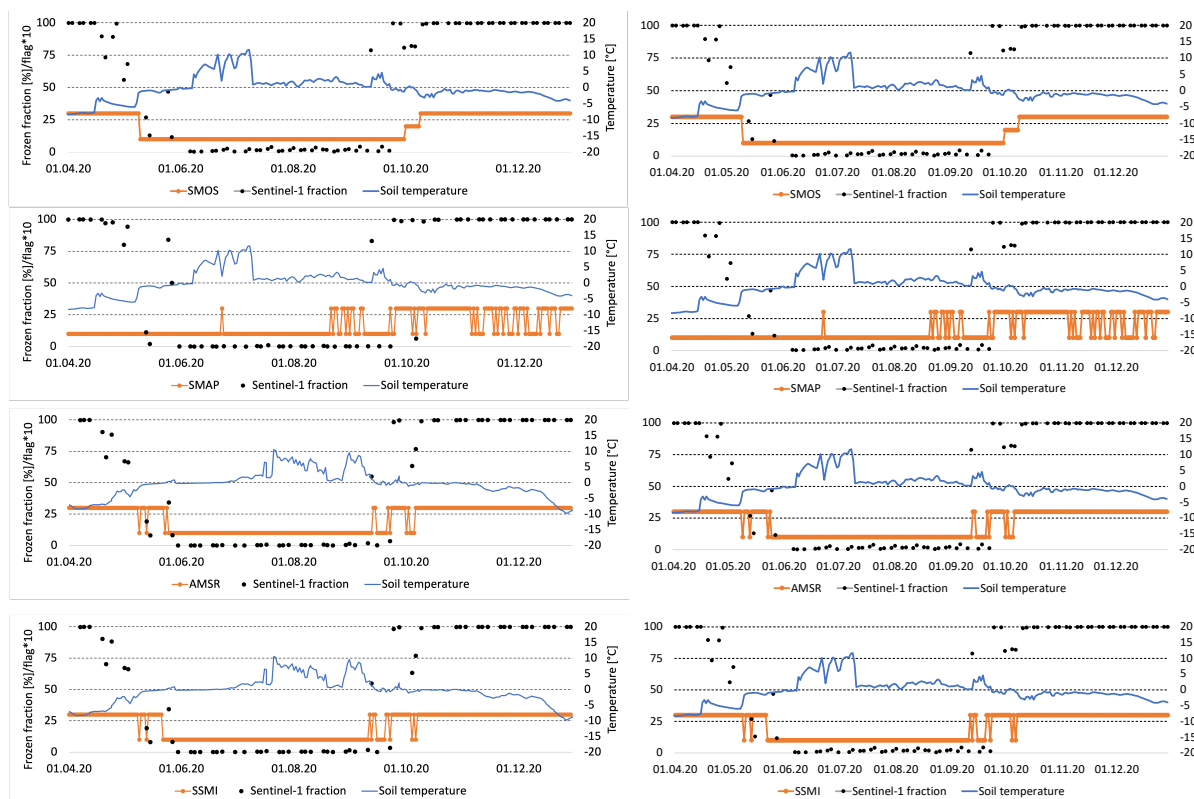


**Figure 8.** Time series for grid cells of passive microwave (PMW) freeze/thaw products (see Table 1) overlapping with the Happy Valley borehole location for 2020 (left) and the Sagwon (SagMNT) borehole location for 2019 (right). Near surface soil temperature (1 cm and 8 cm respectively), Sentinel-1 frozen fraction (differs between PMW datasets due to differing grids) and scaled freeze/thaw flags (10 – unfrozen, 20- partially frozen, 30 – frozen, 0 – no data).

#### 4.5 Assessment of fused records

Records were fused for the same grid cells as for the initial frozen fraction comparison. The assessment procedure followed the same procedure in a first step. The frozen fraction from Sentinel-1 (SMOS grid) was compared by flag and separate for the thaw and freeze-up period.

In addition, the 'partially frozen' flag has been assessed over three selected borehole locations. The frozen fraction for days flagged in the SMOS product were compared to the fused dataset in order to evaluate the added value of MEaSUREs flags. The 'frozen' and 'unfrozen' flag of the fused product was evaluated considering soil temperature as well as reanalyses data (ERA5) at two sites. The latter allows comparison with results of previous studies.



**Table 4.** Fusion scheme recommendation for northern hemisphere. For product details see Table 1. In case of AM/PM data availability, only AM data to be considered.

Period defined by day of year	<210	210 - 300	>300
<b>Input products</b>	MEaSURES (SSMI, AMSR-E) SMOS	MEaSURES (SSMI, AMSR-E) SMAP SMOS	SMOS MEaSURES (SSMI, AMSR-E)
<b>Condition</b>	(1) if one product indicates 'unfrozen' or 'partially frozen' then 'partially frozen', (2) if both indicate 'unfrozen' then 'unfrozen' (3) if both indicate 'frozen' then 'frozen'	(1) if only SMAP 'frozen' then 'partially frozen', (2) if SMAP 'frozen' and (SSMI or AMSR-E or SMOS) 'frozen' then 'frozen' (3) if all 'unfrozen' then 'unfrozen'	either use of SSMI or AMSR-E or SMOS

#### 4.5.1 Alaskan North Slope

The combination of the different products specifically improves the determination of the 'partially frozen' flag for the spring transition (Figure 9). No day with partially frozen conditions was contained in the SMOS product from April to June between 2017 and 2020. This gap can be filled by fusion with the MEaSURES datasets. The majority of grid cells was frozen for days indicated as partially frozen in the SMOS product for August to November for the same years. The fraction distribution is inverted through the fusion with SMAO and MEaSURES (Figure 10). The average frozen fraction for days defined as 'partially frozen' for SMOS is >90% (Table 5). The Sentinel-1 frozen fraction on days with the 'partially frozen' flag after fusion reduces on average to values between 40% and 46 % at the test sites in Alaska (taking spring and autumn into account, Table ). Frozen fraction values are higher in spring than in autumn (Figure 10).

The agreement with near-surface soil temperature records and ERA5 for the frozen and unfrozen flags was similar for the MEaSURES, SMOS and Fusion datasets. In general values were higher for ERA5 (as data represent a grid average), and also similar between sites in this case (appr. 90%, Table 6). The agreement with soil temperature differs between sites and was lower (70-80%). Only SMAP showed a lower agreement for the sites on the Alaskan North Slope, with values ranging between 51 and 72%.

#### 4.5.2 Finland

Partially frozen conditions are also not captured in the SMOS product for April to June at the Northern Finland site when only considering the in situ overlap period 2016 to 2018 (Figure 11) at a site located in a depression (at 337m, with altitude ranging from 200 to more than 400 m in the surroundings). An extensive spring thaw period is identified with the Fusion product in Northern Finland starting early May 2017 (Figure 12). In-situ data from under the snowpack (thick enough to insulate the

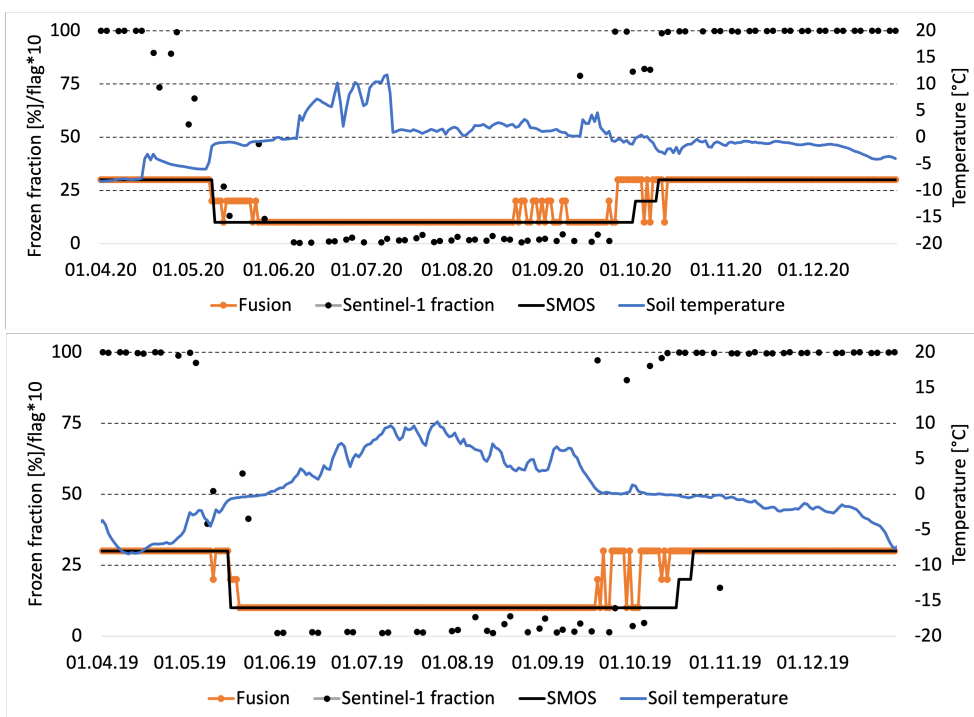


**Figure 9.** Time series example (spring and autumn) of the fused records for the SMOS grid point overlapping with the Happy Valley borehole location for 2020 (top) and the Sagwon borehole location for 2019 (bottom). Near surface soil temperature, Sentinel-1 frozen fraction and scaled freeze/thaw flags for SMOS and Fusion (10 – unfrozen, 20 - partially frozen, 30 – frozen).

**Table 5.** Average Sentinel-1 derived frozen fraction (in %) for footprints of SMOS and the Fusion freeze/thaw state – days with 'partially frozen' flag only. Sample period 2017 to 2020, three sites on Alaskan North Slope. For analyses extent see Figure 2. For product details see Table 1.

Site	SMOS	Fusion
Sagwon	92	46
Happy Valley	91	45
Franklin Bluffs	91	40

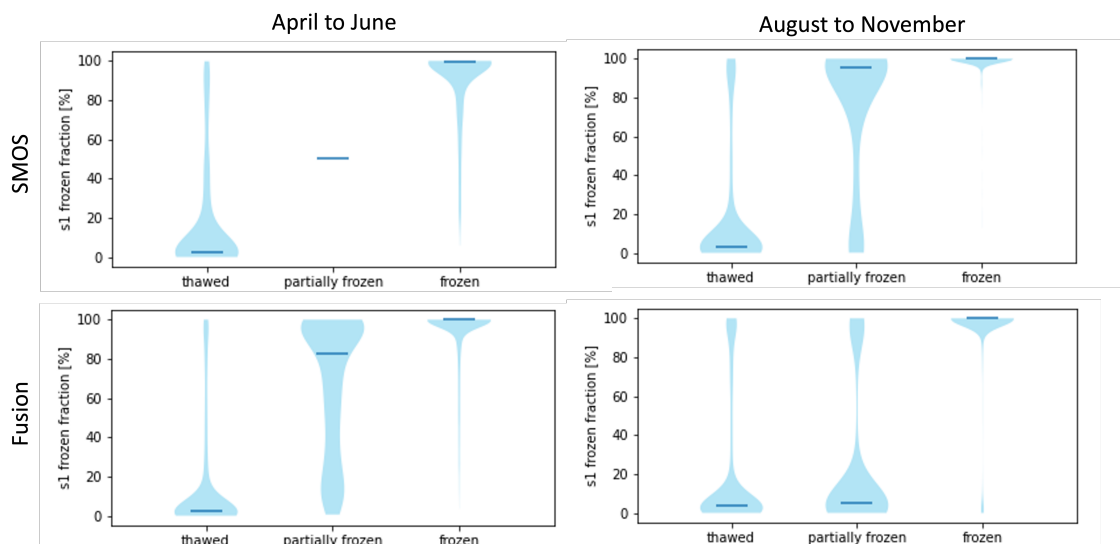


**Figure 10.** Sentinel-1 (s1) derived frozen fraction for footprints of SMOS and the Fusion freeze/thaw state. Sample period 2017 to 2020, Alaskan North Slope. For analyses extent see Figure 2.

**Table 6.** Agreement (in %) of in situ soil temperature and ERA5 temperature derived freeze/thaw states for all products and the Fusion result (gridded to SMOS) – days with 'unfrozen' or 'frozen' flag only. Sample period 2017 to 2020, two sites on Alaskan North Slope. For location of sites see Figure 2. For product details see Table 1.

Site	Type	SSMI	SMOS	SMAP	AMSRE	Fusion
Sagwon	ERA5	92.4	89.2	70.6	92.3	92.7
	Soil	82.6	84.6	60.4	83.2	83.2
Happy Valley	ERA5	92.1	88.3	70.1	90.7	92.8
	Soil	71.8	72.8	51.8	72.0	72.1

355 ground with temperatures remaining at approximately 0°C during the winter and as long as the snow remains) indicate that this period corresponds to snowmelt, instead of near surface soil thaw. The extended period of partially frozen conditions also disagrees with the frozen fraction from Sentinel-1 (Figure 12). SMOS as well as AMSR-E show a high average frozen fraction with 'thawed' (unfrozen) flag over all analysed grid cells (>20%, Figure 11). This also indicates a too early thaw in this region. AMSR-E data was used for the fusion what, however, shifts some of these dates to partially frozen (Figure 12). AMSR-E  
 360 remained unfrozen until the start of the drop of Sentinel-1 frozen fraction in 2017 while SMOS indicated unfrozen conditions since the beginning of May. This disagreement results in 'partially frozen' following the proposed fusion scheme. The end of this period coincided with ERA5 temperature increase above 0°C. The actual end of thaw for the entire grid cell was, however, one month later in early July.

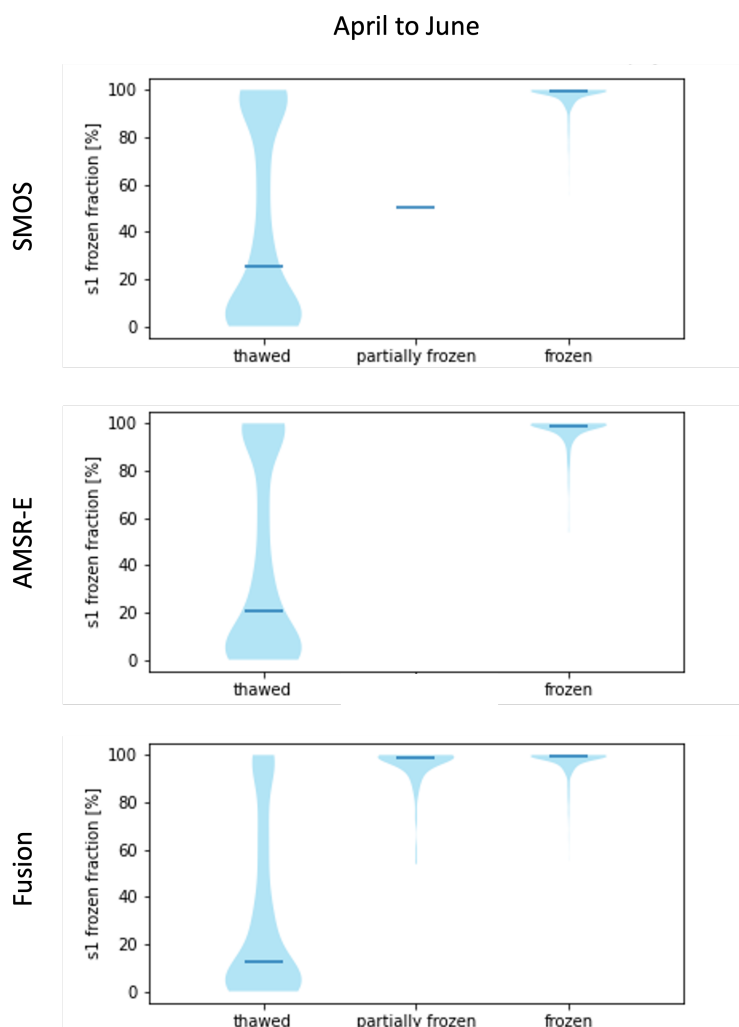


**Figure 11.** Sentinel-1 derived frozen fraction for the Fusion freeze/thaw state (footprints according to SMOS product), Kaldoaivi, Northern Finland. Sample period 2016 to 2018. For analyses area and extent see Figure 2.

365 The Fusion result example in Figure 12 also includes occurrence of mid-winter FT (source: Bartsch et al. (2023b)). The detected events (15.12.2016, 13.02.2017) correspond to periods with ERA5 temperature above 0°C. All analysed PMW products indicate frozen conditions for those dates.

Frozen fraction values on ‘partially frozen’ days are high in spring as well as autumn what differs from the Alaskan North Slope results. But they are lower than in the SMOS product. The fusion reduces the high frozen fraction detection for the  
370 ‘thawed’ state for both, spring and autumn.

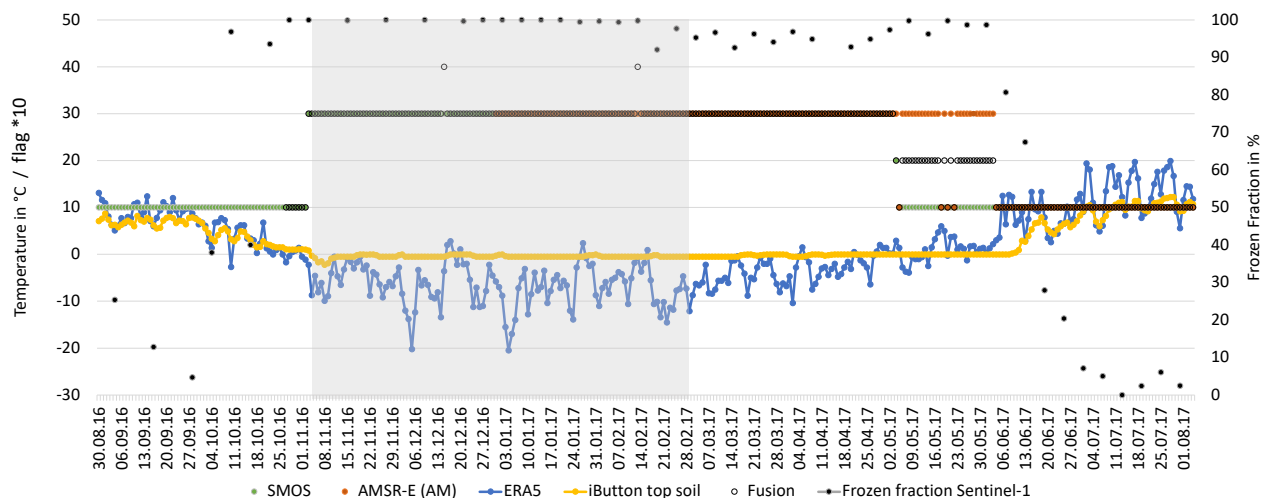


**Figure 12.** Comparison for SMOS grid point overlapping with the Northern Finland site for autumn 2016 and spring 2017 (altitude range 200-400m). Near surface soil temperature (iButton location A4 at 337 m altitude, Bergstedt et al. (2020b)), ERA5 temperature, Sentinel-1 frozen fraction, scaled freeze/thaw flags for SMOS, AMSR-E and Fusion (10 – unfrozen, 20- partially frozen, 30 – frozen, 40 – mid winter thaw and refreeze). The shaded area indicates the analyses period for mid-winter thaw and refreeze (source: Bartsch et al. (2023b)).

## 5 Discussion

### 5.1 Benchmark dataset

The use of combined ratios of backscatter intensity using VV and VH polarization as previously suggested for wet snow detection provides a means of reducing the incidence angle effects, but the impact of temperature variations on backscatter intensity at VV during frozen conditions remains (Figure 3). The combined ratio  $R_C$  also shows this linkage. The potential influence of temperature on FT retrieval at C-VV has been previously discussed (Naeimi et al., 2012; Bergstedt et al., 2018; Bartsch et al., 2023a). Our results demonstrate that this is specific for VV, but not present in VH (Figure 3). The retrieval based on VH alone would, however, require an appropriate approach regarding the influence of the incidence angle, such as normalization of  $\sigma_0$  (Widhalm et al., 2018) or retrieval of  $\gamma_0$  (Small, 2011). An implementation based on VH would also require a location specific threshold determination (instead of global threshold) which is not feasible for the purpose of this study and potential regional application of the FT detection approach.

The combined ratio approach does nevertheless provide good quality results. The overall agreement with in-situ data of 92% at the site in Northern Finland is similar to the previously reported accuracy of 94% using the location (pixel) specific threshold determination approach (Bergstedt et al., 2020b). The validation was carried out over a different region (Northern Finland) than the calibration (Alaskan North Slope) confirming the transferability of the method. The performance is also similar to a CNN (Convolutional Neural Networks) approach using both polarization bands (88%, calibration and validation over same region in



NE Canada, Chen et al. (2024)).

We tested the combined ratio approach only over tundra. It can be expected that the performance is lower over forested regions as it relies on the use of VH. A method as suggested by Cohen et al. (2021) using VV only might perform better for forested areas.

## 5.2 Global/northern hemisphere products benchmarking

The SMOS - Sentinel-1 comparison results agree with findings of Cohen et al. (2021). Offsets in the FT timing compared to in situ measurements were described and attributed to the ability of L-band to represent larger soil depths. SMAP which is also based on L-band, does however, represent the end of the autumn freeze-up period well. The AMSR-E/SSM/I frozen flag indicates also a later freeze-up in some cases (multiple switching from frozen/unfrozen, Figure 8), although a much smaller wavelength is used.

The comparison with the Sentinel-1 frozen fraction and in situ data with the seasonal freeze/thaw prototypes indicates an improvement through the fusion of the different products. A range of issues which differ between the evaluation sites (continuous over Alaska versus sporadic permafrost for Northern Finland), however, remain. Neither the actual end of thaw in spring nor the start of freeze-up in autumn can be captured. These issues cannot be solved based on the existing passive microwave based CDRs.

The frozen fraction derived from Sentinel-1 only applies to areas without open water and barren surfaces. The deviation to the PMW products could therefore also be analysed with respect to open water fraction as has previously investigated for active microwave freeze/thaw Bergstedt et al. (2020a) in order to provide more insight into product issues. An offset in freeze/thaw timing can be expected related to lake ice thaw and formation.

Previous analyses of C-band scatterometer indicated applicability of active microwave data for FT retrieval in high latitude regions (e.g. Naeimi et al. (2012)). Specifically the fusion of SAR and scatterometer is promising for characterization of the transition period (actual determination of start and end, Bergstedt et al. (2020b)). The new SAR based method which has been developed in our study enables operational retrieval of surface state from sensors such as Sentinel-1 and theoretically allows to meet the requirements for a multipurpose FT product if sufficient acquisitions (daily) are available. In addition to soil FT, wet snow detection could be also addressed as it is based on the same pre-processing scheme. The availability of Sentinel-1 data is however constrained and the polarization differs across the Arctic. The required data are unavailable for Greenland and the Canadian High Arctic. In the remaining regions, repeat intervals are not dense enough (daily needed). Bergstedt et al. (2020b) demonstrated, however, the use of historic (one year) Sentinel-1 data for the calibration of a freeze/thaw fraction derived from Metop ASCAT. FT monitoring considering fraction could therefore be implemented in regions with VV/VH availability. Retrieval with HH/HV remains to be tested. An implementation based on Metop ASCAT would allow the production of a CDR



going back to 2012 (Metop A and B availability).

### 5.3 Global/northern hemisphere products utility

Current FT products aim at the identification of an average surface state condition within a footprint (Kim et al. (2014) using  
425 SSMI, Naeimi et al. (2012) using ASCAT, Derksen et al. (2017) using SMAP and Rautiainen et al. (2016) using SMOS),  
but specific applications including permafrost, soil moisture and greenhouse gas fluxes require information on the start of  
thaw/freeze-up and completion of thaw/freeze-up (Tables A1, A2, A3Bartsch et al. (2022)).

#### 5.3.1 Permafrost

Findings for SSMI agree with Kroisleitner et al. (2018). This applies specifically to the observation that the unfrozen period  
430 (complete thaw of grid) in high latitude relatively cold regions is longer than suggested by the benchmarking data (this study,  
Figure 8) and than detected in the experimental product based on Metop ASCAT (Kroisleitner et al., 2018). This impedes  
the applicability for permafrost related applications such as the estimation of potential mean annual ground temperature. The  
impact on the capability to monitor long-term trends (as suggested by Park et al. (2016a)) in frozen period length remains to  
be investigated.

435

Kouki et al. (2019) also compared and evaluated datasets for the start of spring thaw. SSMI/SSMR switch from frozen  
to thawed showed to correspond to the start of increase of temperatures above 0°C what agrees with the Sentinel-1 fraction  
and in situ borehole comparison on the Alaskan North Slope (Figure 8). Results from northern Finland also indicate that the  
frozen/thaw switch (start of decrease of frozen fraction) coincides with increasing air temperatures, but not with upper soil  
440 temperatures (Figure 12). Snow is still present on the ground at this time as indicated through the temperature measurements  
(remains stable close to 0°C) and in situ measurements of snow depth in March 2018 (44 to 86 cm, Bergstedt and Bartsch  
(2020)).

A combination of MEaSUREs (SSMI/AMSR-E) and/or SMOS with SMAP (excluding the winter period) may fulfil the  
445 requirements for a freeze/thaw flag use as proxy for potential permafrost occurrence. Threshold requirements (Table A1) could  
at least be partially met. Diurnal variations may need to be considered with respect to acquisition timing. Freeze/thaw cycles  
on a daily basis have been shown common during the spring period in the context of wet snow detection (e.g. Bartsch et al.,  
2007). This pattern may extent into the snow free period.

Ground temperatures can also be affected by melt of snow in mid-winter (Westermann et al., 2011). Figure 12) provides an  
450 example of an existing microwave remote sensing based product and the co-occurrence of air temperature increase. As near  
surface soil temperatures were already at 0°C in this zone with only sporadic permafrost. A temperature response was thus not  
detected. Previous studies including Westermann et al. (2011) have, however, shown increases in colder regions. A combined  
product is therefore expected to be of benefit for permafrost applications.



### 5.3.2 Masking of soil moisture products

455 With the currently available FT products, target requirements for soil moisture (completely unfrozen determination, Table A2) cannot be met for the transition periods. A partial solution provides the combination of SMOS and MEaSURES for spring thaw. The combination improved the partially frozen flag of SMOS on the Alaskan North Slope (Table 5). Precise determination of start of freeze-up in Autumn based on the existing products is currently not possible.

460 Results of Bergstedt et al. (2020b) indicate that Metop ASCAT backscatter in combination with Sentinel-1 frozen fraction statistics allows to derive start and end of the thaw and freeze transition. A calibration would, however, require the processing of Sentinel-1 for at least one year for each ASCAT footprint to be processed. The frozen fraction could be similarly used for combination with the MEaSURES and SMOS data for the spring period and for defining the start of freeze-up which is not represented yet.

465

### 5.3.3 Vegetation and carbon flux applications

The combination of MEaSURES, SMOS and SMAP is expected to partially fulfil threshold requirements for the classification (Table A3), as the start and end of the transition periods are of relevance in this case. To fulfil the target requirements, also the start of freeze-up would be needed. The consideration of Sentinel-1 facilitated frozen fraction retrieval would be of benefit. AM  
470 and PM information would be eventually required in addition to indication of presence of melting snow in order to monitor diurnal variations which are of relevance for fluxes.

## 6 Conclusions

The joint use of VV and VH available from Sentinel-1 acquisitions has been shown applicable for FT retrieval in high latitudes. This allows for regional scale analyses at comparably high spatial resolution as a global threshold can be defined. The creation  
475 of a freeze/thaw benchmarking dataset requires sufficient temporal sampling at the same time. Both spatial coverage and temporal sampling are major constraints, but implementation based on Sentinel-1 A and B is possible for some regions in the Arctic including Alaska and northern Scandinavia.

For global and northern hemisphere applications coarser resolution datasets such as the tested passive microwave based datasets need to be used at this stage. Improvements of the existing regional to global datasets are, however, needed. The  
480 transition periods are not well captured even when a 'partially frozen' flag, as in case of SMOS, is considered. Such a flag should be (1) included in any future coarse spatial resolution FT product and (2) improved in precision in order to meet various user requirements. A fusion with SAR retrievals may allow to overcome various error sources, specifically seasonally changing water surfaces, which are an issue due to the coarse spatial resolution of PMW observations. The utility of FT datasets could



be further enhanced by combination with wet snow products from direct observations or indirect via snow structure change  
485 resulting from refreezing snow.

A fusion of the existing products can only partially enhance the accuracy. The Sentinel-1 derived benchmark dataset provides a means for improving existing retrieval schemes and the development of new products that so far relied on comparisons with in-situ point or modelled and coarser resolution reanalyses data. Comparison to situ records also need to consider soil temperature measurements in order to evaluate the role of snow.

490 *Author contributions.* AB developed the concept for the study, analysed the results and wrote the first draft of the manuscript. XM, MH and KR have processed the satellite data. JW, TN and KR contributed to the conception of the study and writing of the manuscript. HB and DN contributed to the in situ surveys, their compilation and to the writing of the manuscript.

*Competing interests.* The authors declare no competing interests.

*Acknowledgements.* This work was supported by the European Space Agency CCI+ Permafrost and CCI+ Snow and AMPAC-Net projects.

495 DN acknowledges the US NSF grant 1832238 for supporting his involvement in this study.



## Appendix A: User requirements summary from Bartsch et al. (2022)

**Table A1.** Requirements for a FT climate data record for permafrost monitoring in lowland areas in line with Permafrost\_cci (Bartsch et al., 2023e).

	Threshold requirement	Target requirement
	<b>Coverage and sampling</b>	
<b>Geographical coverage</b>	Pan-Arctic	Global with regional specific products
<b>Temporal sampling</b>	annually (aggregated from daily data)	daily
<b>Temporal extent</b>	Last decade	1979 - present
	<b>Thematic content</b>	
<b>Target classes</b>	frozen, unfrozen	frozen, unfrozen, melting
<b>Accuracy</b>	better accuracy than available so far	<20 % error
	<b>Resolution</b>	
<b>Horizontal resolution</b>	10 km	100m-1km
<b>Subgrid variability</b>	no	yes

**Table A2.** Requirements for a FT climate data record for masking of soil moisture (National Research Council, 2014; Dunbar, 2018; Entekhabi et al., 2014; Trofaier et al., 2017).

	Threshold requirement	Target requirement
	<b>Coverage and sampling</b>	
<b>Geographical coverage</b>	North of 45°N	Global
<b>Temporal sampling</b>	as soil moisture product	daily
<b>Temporal extent</b>	as length of specific mission	1979 - present
	<b>Thematic content</b>	
<b>Target classes</b>	frozen, unfrozen	frozen, partially frozen, unfrozen (complete)
<b>Accuracy</b>	better accuracy than available so far	<20 % error
	<b>Resolution</b>	
<b>Horizontal resolution</b>	as soil moisture product	as soil moisture product
<b>Subgrid variability</b>	no	yes



**Table A3.** Requirements for a FT climate data record for vegetation and carbon flux applications (Böttcher et al., 2018; Bartsch et al., 2007; Aalto et al., 2020).

	Threshold requirement	Target requirement
	<b>Coverage and sampling</b>	
<b>Geographical coverage</b>	Northern hemisphere	Global
<b>Temporal sampling</b>	annually (aggregated from daily data)	diurnal
<b>Temporal extent</b>	Last decade	1979 - present
	<b>Thematic content</b>	
<b>Target classes</b>	start and end day of year of unfrozen period	frozen, partially frozen, unfrozen (complete), melting snow
<b>Accuracy</b>	7.5 days for date of freeze-up, less than 10% of days with missing data	5 days for date of freeze-up
	<b>Resolution</b>	
<b>Horizontal resolution</b>	1°	100m-25 km
<b>Subgrid variability</b>	yes	yes

## References

- Aalto, T., Lindqvist, H., Tsuruta, A., Tenkanen, M., Karppinen, T., Kivimäki, E., Smolander, T., Kangasaho, V., and K., R.: ESA MethEO Final Report, Tech. rep., FMI, [https://eo4society.esa.int/wp-content/uploads/2021/02/MethEO\\_Final-Report\\_v1\\_0.pdf](https://eo4society.esa.int/wp-content/uploads/2021/02/MethEO_Final-Report_v1_0.pdf), 2020.
- 500 Bartsch, A., Kidd, R. A., Wagner, W., and Bartalis, Z.: Temporal and Spatial Variability of the Beginning and End of Daily Spring Freeze/Thaw Cycles Derived from Scatterometer Data, *Remote Sensing of Environment*, 106, 360–374, <https://doi.org/10.1016/j.rse.2006.09.004>, 2007.
- Bartsch, A., Pointner, G., Bergstedt, H., Widhalm, B., Wendleder, A., and Roth, A.: Utility of Polarizations Available from Sentinel-1 for Tundra Mapping, in: 2021 IEEE International Geoscience and Remote Sensing Symposium IGARSS, IEEE, 505 <https://doi.org/10.1109/igarss47720.2021.9553993>, 2021a.
- Bartsch, A., Pointner, G., Nitze, I., Efimova, A., Jakober, D., Ley, S., Högström, E., Grosse, G., and Schweitzer, P.: Expanding infrastructure and growing anthropogenic impacts along Arctic coasts, *Environmental Research Letters*, 16, 115 013, <https://doi.org/10.1088/1748-9326/ac3176>, 2021b.
- Bartsch, A., Nagler, T., Wuite, J., Rautiainen, K., and Strozzi, T.: Towards a multipurpose freeze/thaw CDR - D1.1 User Requirement Document (URD), Tech. rep., [https://climate.esa.int/documents/1653/CCI\\_PERMA\\_CCN3O3\\_D1.1\\_URD\\_v1.0.pdf](https://climate.esa.int/documents/1653/CCI_PERMA_CCN3O3_D1.1_URD_v1.0.pdf), 2022.
- 510 Bartsch, A., Bergstedt, H., Pointner, G., Muri, X., and Rautiainen, K.: Circumpolar mid-winter thaw and refreeze based on fusion of Metop ASCAT and SMOS, 2011/2012 - 2021/2022, <https://doi.org/10.5281/ZENODO.7575927>, 2023a.
- Bartsch, A., Bergstedt, H., Pointner, G., Muri, X., Rautiainen, K., Leppänen, L., Joly, K., Sokolov, A., Orekhov, P., Ehrich, D., and Soininen, E. M.: Towards long-term records of rain-on-snow events across the Arctic from satellite data, *The Cryosphere*, 17, 889–915, 515 <https://doi.org/10.5194/tc-17-889-2023>, 2023b.



- Bartsch, A., Efimova, A., Widhalm, B., Muri, X., von Baeckmann, C., Bergstedt, H., Ermokhina, K., Hugelius, G., Heim, B., and Leibmann, M.: Circumpolar Landcover Units, <https://doi.org/10.5281/ZENODO.8399017>, 2023c.
- Bartsch, A., Efimova, A., Widhalm, B., Muri, X., von Baeckmann, C., Bergstedt, H., Ermokhina, K., Hugelius, G., Heim, B., and Leibmann, M.: Circumarctic landcover diversity considering wetness gradients, <https://doi.org/10.5194/egusphere-2023-2295>, 2023d.
- 520 Bartsch, A., Matthes, H., Westermann, S., Heim, B., Pellet, C., Onacu, A., Kroisleitner, C., and Strozzi, T.: ESA CCI+ Permafrost User Requirements Document, v3.0, Tech. rep., [https://climate.esa.int/documents/2137/CCI\\_PERMA\\_URD\\_v3.0.pdf](https://climate.esa.int/documents/2137/CCI_PERMA_URD_v3.0.pdf), 2023e.
- Bergstedt, H. and Bartsch, A.: Surface State across Scales; Temporal and Spatial Patterns in Land Surface Freeze/Thaw Dynamics, *Geosciences*, 7, 65, <https://doi.org/10.3390/geosciences7030065>, 2017.
- Bergstedt, H. and Bartsch, A.: Near surface ground temperature, soil moisture and snow depth measurements in the Kaldoaivi Wilderness  
525 Area, for 2016-2018, <https://doi.org/10.1594/PANGAEA.912482>, 2020.
- Bergstedt, H., Zwieback, S., Bartsch, A., and Leibman, M.: Dependence of C-Band Backscatter on Ground Temperature, Air Temperature and Snow Depth in Arctic Permafrost Regions, *Remote Sensing*, 10, <https://doi.org/10.3390/rs10010142>, 2018.
- Bergstedt, H., Bartsch, A., Duguay, C. R., and Jones, B. M.: Influence of surface water on coarse resolution C-band backscatter: Implications for freeze/thaw retrieval from scatterometer data, *Remote Sensing of Environment*, 247, 111911,   
530 <https://doi.org/10.1016/j.rse.2020.111911>, 2020a.
- Bergstedt, H., Bartsch, A., Neureiter, A., Hofler, A., Widhalm, B., Pepin, N., and Hjort, J.: Deriving a Frozen Area Fraction From Metop ASCAT Backscatter Based on Sentinel-1, *IEEE Transactions on Geoscience and Remote Sensing*, 58, 6008–6019, <https://doi.org/10.1109/tgrs.2020.2967364>, 2020b.
- Biskaborn, B. K., Smith, S. L., Noetzli, J., Matthes, H., Vieira, G., Streletskiy, D. A., Schoeneich, P., Romanovsky, V. E., Lewkowicz, A. G.,  
535 Abramov, A., Allard, M., Boike, J., Cable, W. L., Christiansen, H. H., Delaloye, R., Diekmann, B., Drozdov, D., Eitzelmüller, B., Grosse, G., Guglielmin, M., Ingeman-Nielsen, T., Isaksen, K., Ishikawa, M., Johansson, M., Johannsson, H., Joo, A., Kaverin, D., Kholodov, A., Konstantinov, P., Krüger, T., Lambiel, C., Lanckman, J.-P., Luo, D., Malkova, G., Meiklejohn, I., Moskalenko, N., Oliva, M., Phillips, M., Ramos, M., Sannel, A. B. K., Sergeev, D., Seybold, C., Skryabin, P., Vasiliev, A., Wu, Q., Yoshikawa, K., Zheleznyak, M., and Lantuit, H.: Permafrost is warming at a global scale, *Nature Communications*, 10, <https://doi.org/10.1038/s41467-018-08240-4>, 2019.
- 540 Böttcher, K., Rautiainen, K., Aurela, M., Kolari, P., Mäkelä, A., Arslan, A. N., Black, T. A., and Koponen, S.: Proxy Indicators for Mapping the End of the Vegetation Active Period in Boreal Forests Inferred from Satellite-Observed Soil Freeze and ERA-Interim Reanalysis Air Temperature, *PFG- Journal of Photogrammetry, Remote Sensing and Geoinformation Science*, 86, 169–185, <https://doi.org/10.1007/s41064-018-0059-y>, 2018.
- Chen, X., Liu, L., and Bartsch, A.: Detecting soil freeze/thaw onsets in Alaska using SMAP and ASCAT data, *Remote Sensing of Environ-*  
545 *ment*, 220, 59–70, <https://doi.org/10.1016/j.rse.2018.10.010>, 2019.
- Chen, Y., Li, S., Wang, L., Mittermeier, M., Bernier, M., and Ludwig, R.: Retrieving freeze-thaw states using deep learning with remote sensing data in permafrost landscapes, *International Journal of Applied Earth Observation and Geoinformation*, 126, 103616, <https://doi.org/10.1016/j.jag.2023.103616>, 2024.
- Cohen, J., Rautiainen, K., Lemmetyinen, J., Smolander, T., Vehviläinen, J., and Pulliainen, J.: Sentinel-1 based soil freeze/thaw estimation  
550 in boreal forest environments, *Remote Sensing of Environment*, 254, 112267, <https://doi.org/10.1016/j.rse.2020.112267>, 2021.
- Derksen, C., Xu, X., Dunbar, R. S., Colliander, A., Kim, Y., Kimball, J. S., Black, T. A., Euskirchen, E., Langlois, A., Loranty, M. M., Marsh, P., Rautiainen, K., Roy, A., Royer, A., and Stephens, J.: Retrieving landscape freeze/thaw state from Soil Moisture Active Passive (SMAP) radar and radiometer measurements, *Remote Sensing of Environment*, 194, 48–62, <https://doi.org/10.1016/j.rse.2017.03.007>, 2017.



- 555 Dodd, E., Ermida, S., Jimenez, C., Martin, M., and Ghent, D.: Data Access Requirements Document: WP1.3-LST-CCI-D1.3, Tech. rep., Consortium CCI LST, [https://admin.climate.esa.int/media/documents/LST-CCI-D1.3-DARD\\_-\\_i2r0\\_-\\_Data\\_Access\\_Requirements\\_Document.pdf](https://admin.climate.esa.int/media/documents/LST-CCI-D1.3-DARD_-_i2r0_-_Data_Access_Requirements_Document.pdf), 2021.
- Dunbar, R. S.: Soil Moisture Active Passive (SMAP) Mission - Level 3 Freeze-Thaw Passive Product Specification Document, Tech. Rep. JPL D-56293, [https://nsidc.org/sites/default/files/d-56293\\_smap2013\\_ft\\_p20psd\\_05312018.pdf](https://nsidc.org/sites/default/files/d-56293_smap2013_ft_p20psd_05312018.pdf), 2018.
- 560 Entekhabi, D., Yueh, S., O'Neill, P. E., Kellogg, K. H., Allen, A., Bindlish, R., Brown, M., Chan, S., Colliander, A., Crow, W. T., Das, N., De Lannoy, G., Dunbar, R. S., Edelstein, W. N., Entin, J. K., Escobar, V., Goodman, S. D., Jackson, T. J., Jai, B., Johnson, J., Kim, E., Kim, S., Kimball, J., Koster, R. D., Leon, A., McDonald, K. C., Moghaddam, M., Mohammed, P., Moran, S., Njoku, E. G., Piepmeier, J. R., Reichle, R., Rogez, F., Shi, J., Spencer, M. W., Thurman, S. W., Tsang, L., Van Zyl, J., Weiss, B., and West, R.: SMAP Handbook-Soil Moisture Active Passive: Mapping Soil Moisture and Freeze/Thaw from Space, [https://smap.jpl.nasa.gov/files/smap2/SMAP\\_handbook\\_web.pdf](https://smap.jpl.nasa.gov/files/smap2/SMAP_handbook_web.pdf), 2014.
- 565 Erkkilä, A., Tenkanen, M., Tsuruta, A., Rautiainen, K., and Aalto, T.: Environmental and Seasonal Variability of High Latitude Methane Emissions Based on Earth Observation Data and Atmospheric Inverse Modelling, *Remote Sensing*, 15, 5719, <https://doi.org/10.3390/rs15245719>, 2023.
- Johnston, J., Maggioni, V., and Houser, P.: Comparing global passive microwave freeze/thaw records: Investigating differences between Ka- and L-band products, *Remote Sensing of Environment*, 247, 111 936, <https://doi.org/10.1016/j.rse.2020.111936>, 2020.
- 570 Jorgenson, M. T., Yoshikawa, K., Kanevskiy, M., Shur, Y., Romanovsky, V., Marchenko, S., Grosse, G., Brown, J., and Jones, B.: Permafrost characteristics of Alaska, in: *Proceedings of the Ninth International Conference on Permafrost*, pp. 121–122, University of Alaska, Fairbanks, AK, 2008.
- Kim, Y., Kimball, J. S., Zhang, K., and McDonald, K. C.: Satellite detection of increasing Northern Hemisphere non-frozen seasons from 1979 to 2008: Implications for regional vegetation growth, *Remote Sensing of Environment*, 121, 472–487, <https://doi.org/10.1016/j.rse.2012.02.014>, 2012.
- 575 Kim, Y., Kimball, J. S., Glassy, J., and McDonald, K. C.: MEaSUREs Global Record of Daily Landscape Freeze/Thaw Status, Version 3, <https://doi.org/10.5067/MEASURES/CRYOSPHERE/nsidc-0477.003>, 2014.
- Kim, Y., Kimball, J. S., Glassy, J., and Du, J.: An extended global Earth system data record on daily landscape freeze-thaw status determined from satellite passive microwave remote sensing, *Earth System Science Data*, 9, 133–147, <https://doi.org/10.5194/essd-9-133-2017>, 2017.
- 580 Kim, Y., Kimball, J. S., Du, J., Schaaf, C. L. B., and Kirchner, P. B.: Quantifying the effects of freeze-thaw transitions and snowpack melt on land surface albedo and energy exchange over Alaska and Western Canada, *Environmental Research Letters*, 13, 075 009, <https://doi.org/10.1088/1748-9326/aac72>, 2018.
- Kim, Y., Kimball, J. S., Parazoo, N., and Kirchner, P.: Diagnosing Environmental Controls on Vegetation Greening and Browning Trends Over Alaska and Northwest Canada Using Complementary Satellite Observations, pp. 583–613, Springer International Publishing, ISBN 9783030509309, [https://doi.org/10.1007/978-3-030-50930-9\\_20](https://doi.org/10.1007/978-3-030-50930-9_20), 2020.
- 585 Kim, Y., Kimball, J., Glassy, J., and McDonald, K.: MEaSUREs Northern Hemisphere Polar EASE-Grid 2.0 Daily 6 km Land Freeze/Thaw Status from AMSR-E and AMSR2, Version 2, <https://doi.org/10.5067/BDY2V548E07C>, 2021.
- Kouki, K., Anttila, K., Manninen, T., Luojus, K., Wang, L., and Riihelä, A.: Intercomparison of Snow Melt Onset Date Estimates From Optical and Microwave Satellite Instruments Over the Northern Hemisphere for the Period 1982–2015, *Journal of Geophysical Research: Atmospheres*, 124, 11 205–11 219, <https://doi.org/10.1029/2018jd030197>, 2019.
- 590



- Kraatz, S., Jacobs, J., Schrder, R., Cho, E., Cosh, M., Seyfried, M., Prueger, J., and Livingston, S.: Evaluation of SMAP Freeze/Thaw Retrieval Accuracy at Core Validation Sites in the Contiguous United States, *Remote Sensing*, 10, 1483, <https://doi.org/10.3390/rs10091483>, 2018.
- Kroisleitner, C., Bartsch, A., and Bergstedt, H.: Circumpolar patterns of potential mean annual ground temperature based on surface state obtained from microwave satellite data, *The Cryosphere*, 12, 2349–2370, <https://doi.org/10.5194/tc-12-2349-2018>, 2018.
- 595 Naeimi, V., Paulik, C., Bartsch, A., Wagner, W., Kidd, R., Park, S. E., Elger, K., and Boike, J.: ASCAT Surface State Flag (SSF): Extracting Information on Surface Freeze/Thaw Conditions From Backscatter Data Using an Empirical Threshold-Analysis Algorithm, *IEEE Transactions on Geoscience and Remote Sensing*, 50, 2566–2582, <https://doi.org/10.1109/TGRS.2011.2177667>, 2012.
- Nagler, T. and Rott, H.: Retrieval of Wet Snow by Means of Multitemporal SAR Data, *IEEE Transactions on Geoscience and Remote Sensing*, 38, 754–765, 2000.
- 600 Nagler, T., Rott, H., Ripper, E., Bippus, G., and Hetzenecker, M.: Advancements for Snowmelt Monitoring by Means of Sentinel-1 SAR, *Remote Sensing*, 8, 348, <https://doi.org/10.3390/rs8040348>, 2016.
- National Research Council: Opportunities to Use Remote Sensing in Understanding Permafrost and Related Ecological Characteristics: Report of a Workshop, National Academies Press, Washington, DC, ISBN 9780309301213, <https://doi.org/10.17226/18711>, 2014.
- Outcalt, S. I., Nelson, F. E., and Hinkel, K. M.: The zero-curtain effect: Heat and mass transfer across an isothermal region in freezing soil, *Water Resources Research*, 26, 1509–1516, <https://doi.org/10.1029/wr026i007p01509>, 1990.
- 605 Park, H., Kim, Y., and Kimball, J.: Widespread permafrost vulnerability and soil active layer increases over the high northern latitudes inferred from satellite remote sensing and process model assessments, *Remote Sensing of Environment*, pp. 349–358, <https://doi.org/10.1016/j.rse.2015.12.046>, 2016a.
- Park, H., Yoshikawa, Y., Oshima, K., Kim, Y., Ngo-Duc, T., Kimball, J. S., and Yang, D.: Quantification of Warming Climate-Induced Changes in Terrestrial Arctic River Ice Thickness and Phenology, *Journal of Climate*, 29, 1733–1754, <https://doi.org/10.1175/JCLI-D-15-0569.1>, 2016b.
- 610 Park, S.-E., Bartsch, A., Sabel, D., Wagner, W., Naeimi, V., and Yamaguchi, Y.: Monitoring Freeze/Thaw Cycles Using ENVISAT ASAR Global Mode, *Remote Sensing of Environment*, 115, 3457–3467, <https://doi.org/10.1016/j.rse.2011.08.009>, 2011.
- Park, T., Ganguly, S., Tommervik, H., Euskirchen, E. S., Hogda, K.-A., Karlsen, S. R., Brovkin, V., Nemani, R. R., and Myneni, R. B.: Changes in growing season duration and productivity of northern vegetation inferred from long-term remote sensing data, *Environmental Research Letters*, 11, 084001, <https://doi.org/10.1088/1748-9326/11/8/084001>, 2016c.
- 615 Paulik, C., Melzer, T., Hahn, S., Bartsch, A., Heim, B., Elger, K., and Wagner, W.: Circumpolar surface soil moisture and freeze/thaw surface status remote sensing products (Version 2) with links to geotiff images and NetCDF files (2007-01 to 2010-09), <https://doi.org/10.1594/PANGAEA.775959>, 2012.
- 620 Rautiainen, K., Parkkinen, T., Lemmetyinen, J., Schwank, M., Wiesmann, A., Ikonen, J., Derksen, C., Davydov, S., Davydova, A., Boike, J., Langer, M., Drusch, M., and Pulliainen, J.: SMOS prototype algorithm for detecting autumn soil freezing, *Remote Sensing of Environment*, 180, 346–360, <https://doi.org/10.1016/j.rse.2016.01.012>, 2016.
- Rixen, C., Hye, T. T., Macek, P., Aerts, R., Alatalo, J. M., Anderson, J. T., Arnold, P. A., Barrio, I. C., Bjerke, J. W., Bjrkman, M. P., Blok, D., Blume-Werry, G., Boike, J., Bokhorst, S., Carbognani, M., Christiansen, C. T., Convey, P., Cooper, E. J., Cornelissen, J. H. C., Coulson, S. J., Dorrepaal, E., Elberling, B., Elmendorf, S. C., Elphinstone, C., Forte, T. G., Frei, E. R., Geange, S. R., Gehrmann, F., Gibson, C., Grogan, P., Halbritter, A. H., Harte, J., Henry, G. H., Inouye, D. W., Irwin, R. E., Jespersen, G., Jr, I. S., Jung, J. Y., Klingses, D. H., Kudo, G., L., Lee, H., Lembrechts, J. J., Lett, S., Lynn, J. S., Mann, H. M., Mastepanov, M., Morse, J., Myers-Smith, I. H., Olofsson, J., Paavola, R., Petraglia, A., Phoenix, G. K., Semenchuk, P., Siewert, M. B., Slatyer, R., Spasojevic, M. J., Suding, K., Sullivan, P., Thompson, K. L.,



- Vn, M., Vandvik, V., Venn, S., Walz, J., Way, R., Welker, J. M., Wipf, S., and Zong, S.: Winters are changing: snow effects on Arctic and alpine tundra ecosystems, *Arctic Science*, 8, 572–608, <https://doi.org/10.1139/as-2020-0058>, 2022.
- 630 Small, D.: Flattening Gamma: Radiometric Terrain Correction for SAR Imagery, *IEEE Transactions on Geoscience and Remote Sensing*, 49, 3081–3093, <https://doi.org/10.1109/tgrs.2011.2120616>, 2011.
- Smith, A., Jahn, A., Burgard, C., and Notz, D.: Improving model-satellite comparisons of sea ice melt onset with a satellite simulator, *The Cryosphere*, 16, 3235–3248, <https://doi.org/10.5194/tc-16-3235-2022>, 2022.
- 635 Tenkanen, M., Tsuruta, A., Rautiainen, K., Kangasaho, V., Ellul, R., and Aalto, T.: Utilizing Earth Observations of Soil Freeze/Thaw Data and Atmospheric Concentrations to Estimate Cold Season Methane Emissions in the Northern High Latitudes, *Remote Sensing*, 13, 5059, <https://doi.org/10.3390/rs13245059>, 2021.
- Trofaier, A. M., Westermann, S., and Bartsch, A.: Progress in space-borne studies of permafrost for climate science: Towards a multi-ECV approach, *Remote Sensing of Environment*, 203, 55–70, <https://doi.org/10.1016/j.rse.2017.05.021>, 2017.
- 640 Westermann, S., Boike, J., Langer, M., Schuler, T. V., and Eitzelmüller, B.: Modeling the impact of wintertime rain events on the thermal regime of permafrost, *The Cryosphere*, 5, 945–959, <https://doi.org/10.5194/tc-5-945-2011>, 2011.
- Widhalm, B., Bartsch, A., and Goler, R.: Simplified Normalization of C-Band Synthetic Aperture Radar Data for Terrestrial Applications in High Latitude Environments, *Remote Sensing*, 10, <https://doi.org/10.3390/rs10040551>, 2018.
- Zhang, C., Douglas, T. A., and Anderson, J. E.: Modeling and mapping permafrost active layer thickness using field measurements and remote sensing techniques, 102, 102455, <https://doi.org/10.1016/j.jag.2021.102455>, 2021.
- 645 Zhong, W., Yuan, Q., Liu, T., and Yue, L.: Freeze/thaw onset detection combining SMAP and ASCAT data over Alaska: A machine learning approach, *Journal of Hydrology*, 605, 127354, <https://doi.org/10.1016/j.jhydrol.2021.127354>, 2022.